DOKUZ EYLÜL UNIVERSITY

GRADUATE SCHOOL OF NATURAL AND APPLIED SCIENCES

PRODUCTION AND DEVELOPMENT OF LIGHT METAL CONTAINING HIGH ENTROPY ALLOYS BY A SELF-PROPAGATING HIGH-TEMPERATURE SYNTHESIS METHOD

by

Aslıhan KARAKANAT

September, 2022

İZMİR

PRODUCTION AND DEVELOPMENT OF LIGHT METAL CONTAINING HIGH ENTROPY ALLOYS BY A SELF-PROPAGATING HIGH-TEMPERATURE SYNTHESIS METHOD

A Thesis Submitted to the

Graduate School of Natural and Applied Sciences of Dokuz Eylül University

in Partial Fulfillment of the Requirements for the Degree of Master of

Science in Metallurgical and Materials Engineering, Metallurgical and

Materials Engineering Program

by

Aslıhan KARAKANAT

September, 2022

İZMİR

M.Sc THESIS EXAMINATION RESULT FORM

We have read the thesis entitled "**PRODUCTION AND DEVELOPMENT OF LIGHT METAL CONTAINING HIGH ENTROPY ALLOYS BY A SELF-PROPAGATING HIGH-TEMPERATURE SYNTHESIS METHOD**" completed by **ASLIHAN KARAKANAT** under supervision of **ASSOC. PROF. DR. ESRA DOKUMACI ALKAN**, and we certify that, in our opinion, it is fully adequate, in scope and quality, as a thesis for the degree of Master of Science.

……

Assoc. Prof. Dr. Esra DOKUMACI ALKAN

Supervisor

……	…..……
Assist. Prof. Dr. Murat ALKAN	**Assoc. Prof. Dr. Mehmet BUĞDAYCI**
(Jury Member)	**(Jury Member)**

Prof. Dr. Okan FISTIKOĞLU

Director

Graduate School of Natural and Applied Sciences

ACKNOWLEDGEMENTS

In the realization of this study, first and uppermost, I would like to express my gratitude and respect to Assoc. Prof. Esra DOKUMACI ALKAN, who shared her valuable knowledge and experiences with me and guided me, did not spare me her smiling face and sincerity.

In order to thank Dr. Murat ALKAN for his assistance with my 2018 Undergraduate Graduation Project and Master Thesis, I would like to say that I appreciate all of his time, advice, and support. I would also like to thank Research Assistants Orkut SANCAKOĞLU and Ramazan DALMIŞ, who helped me with their support and contributions throughout my Master's Thesis.

I would like to thank TUBITAK (The Scientific and Technological Research Council of Turkey, Project No. 118M204) for the financial support for this research throughout my Master's Thesis. I would also like to thank MTA (General Directorate of Mineral Research and Exploration) for assistance in chemical analysis.

I would like to owe my special thanks to my dear friend Dilan UĞURLUER, with whom we overcame the difficulties together in my undergraduate and graduate studies. She was with me not only at university in every aspect of my life and was one of the most beautiful people I have met throughout my university life. We supported each other in every situation. I would also like to thank Research Assistant Saadet GÜLER for his help in our study.

I would like to express my deepest gratitude to my dear mother Ayten ÇOTUK, and my dear father Ramazan KARA. They always supported me throughout my life, thought of me before themselves, and were always there for me in all my difficult times. I would like to thank so much my dear sister Neslihan KÖSE and my brother M.Tolgahan KARA, who have always been with me and supported me throughout my life. Finally and deeply, I would like to owe my special thanks to my dear husband, Eren KARAKANAT, who has always been with me throughout my graduate education and my life and has never spared her love and support.

Aslıhan KARAKANAT

PRODUCTION AND DEVELOPMENT OF LIGHT METAL CONTAINING HIGH ENTROPY ALLOYS BY SELF-PROPAGATING HIGH-TEMPERATURE SYNTHESIS METHOD

ABSTRACT

In this study, self-propagating high-temperature synthesis (SHS), a highly energy-efficient, fast, and affordable production technique, was used to create light metal alloys with high entropy that are based on $AlSiTiME_IME_{II}$ (ME_I, ME_{II} = Mg, Nb, V, Mn, Cr, Fe). Experimental studies for obtaining L-HEAs can be divided into Thermodynamic Investigation, SHS Experiments, and Characterization. This study aims to get general information about LHEAs, determine the target alloy systems, and produce and characterize the final products. Metal oxide powders (TiO_2, V_2O_5, Nb_2O_5, MnO_2, Cr_2O_3, CrO_3, Fe_2O_3) and reductants (metallic Al, Si, and Mg powders) were the primary ingredients employed in the SHS studies. The raw material mixtures were prepared as 150-200g, and SHS experiments were carried out. The alloy systems were determined following the results of the Thermodynamic Analysis, which constitutes the first stage of the thesis study. The microstructure and mechanical properties of obtained L-HEAs were investigated through extensive characterization studies with scanning electron microscopy (SEM), X-ray diffraction (XRD), X-ray fluorescence (XRF), and microhardness test device.

As a result of the characterization studies, it has been observed that the L-HEAs are composed of multi-phase microstructures. Furthermore, there are casting cavities in the structure of L-HEAs. In future work on this Thesis study, the search for the impact of heat treatment and secondary melting process in these alloy systems is planned. This study also contributed to establishing a scientific and engineering background of a project performed by TUBITAK (The Scientific and Technological Research Council of Turkey, Project No. 118M204).

Keywords: Light metals, Light-weight high entropy alloy, Self-propagating high-temperature synthesis

KENDİLİĞİNDEN İLERLEYEN YÜKSEK SICAKLIK SENTEZİ YÖNTEMİ İLE HAFİF METAL İÇERİKLİ YÜKSEK ENTROPİLİ ALAŞIMLARIN ÜRETİLMESİ VE GELİŞTİRİLMESİ

ÖZ

Bu çalışmada, yüksek enerji verimli, hızlı ve düşük maliyetli bir üretim tekniği olan kendiliğinden ilerleyen yüksek sıcaklık sentezi (SHS) yöntemi kullanılarak $AlSiTiME_IME_{II}$ (ME_I, ME_{II} = Mg, Nb, V, Mn, Cr, Fe) hafif metal içeren yüksek etnropili alaşımlar (L-HEAs) üretilmiştir. Bu çalışma kapsamında, LHEA'lar hakkında genel bilgilerin elde edilmesi, hedef alaşım sistemlerinin belirlenmesi, nihai ürünlerin üretilmesi ve karakterize edilmesi amaçlanmıştır. L-HEA'ların üretimi için deneysel çalışmalar Termodinamik Analiz, SHS Reaksiyonları ve Ürünlerin Karakterizasyonu olmak üzere üç bölüme ayrılabilir.

Tez çalışmasının ilk aşamasını oluşturan Termodinamik incelemeler sonucunda alaşım sistemleri belirlenmiştir. SHS deneylerinde çeşitli metal oksit tozları (TiO_2, V_2O_5, Nb_2O_5, MnO_2, Cr_2O_3, CrO_3 ve Fe_2O_3) ve indirgeyici metalik tozlar (Al, Si ve Mg) kullanılmıştır. Hammadde toz karışımları 150-200g olarak hazırlanmış ve deneyler gerçekleştirilmiştir. Ürünler, karakterizasyon çalışmaları için hazırlanmıştır. L-HEA'ların mikroyapısı ve mekanik özellikleri, taramalı elektron mikroskobu (SEM), X-ışını difraksiyonu (XRD), X-ışını floresans (XRF) ve mikrosertlik (mikro-vickers) test cihazı ile gerçekleştirilen kapsamlı karakterizasyon çalışmaları yoluyla incelenmiştir. Bu çalışmalar sonucunda, L-HEA'ların çok fazlı mikroyapılardan oluştuğu ve yapısında döküm boşlukları bulunduğu gözlenmiştir. Isıl işlem ve ikincil ergitme işleminin bu alaşımlar üzerindeki etkisinin araştırılması gelecekte yapılması planlanan çalışmalardır. Bu çalışma, aynı zamanda TÜBİTAK (Türkiye Bilimsel ve Teknolojik Araştırma Kurumu, Proje No:118M204) tarafından yürütülen bir projenin bilimsel ve mühendislik altyapısının oluşturulmasına da katkıda bulunulmuştur.

Anahtar kelimeler: Hafif metaller, Hafif yüksek entropi alaşımı, Kendiliğinden ilerleyen yüksek sıcaklık sentezi

CONTENTS

Page

LIST OF FIGURES

Page

LIST OF TABLES

Page

LIST OF SYMBOLS

K	: Kelvin
k_B	: Boltzman constant, 1.38 x10^{-23} J/K
S	: Entropy
ΔG_{mix}	: Gibbs Energy of Mixing
ΔH_{mix}	: Enthalpy of Mixing
ΔS_{mix}	: Entropy of Mixing
T	: Temperature
ΔS_{conf}	: Configurational Entropy of a System
R	: Molar Gas Constant
MPa	: MegaPascal
HV	: Vickers Hardness
^oC	: Celsius
F	: Freedom Degrees
C	: Count of Components
P	: Count of Phases
GPa	: GigaPascal
T_0	: Initial Temperature
T_{ig}	: Ignition Temperature
T_{ad}	: Adiabatic Temperature
T_c	: Actual Combustion Temperature
$\Delta G°$	: Standard Free Energy Change
$\Delta H°$	: Standard Enthalpy Change
$\Delta S°$	: Standard Entropy Change
C_p	: Specific Heat
K_{eq}	: Solution Constant
$[D_{Me}]$	: distribution ratio of metal in alloy
(D_{Me})	: distribution ratio of metal in slag

ABBREVIATIONS

HEA	: High Entropy Alloy
L-HEAs	: Light Metal Containing High Entropy Alloys
SHS	: Self-Propagating High-Temperature Synthesis
SEM	: Scanning Electron Microscopy
XRD	: X-Ray Diffraction
XRF	: X-Ray Fluorescence
MPEAs	: Multi-Principal Element Alloys
FCC	: Face-Centered Cubic
BCC	: Body-Centered Cubic
R-HEAs	: High Entropy Refractory Metal Alloys
HE-BMGs	: High Entropy Bulk Metallic Glasses
HESAs	: High Entropy Superalloys
HCP	: Hexagonal Close-Packed
DSC	: Differential Scanning Calorimetry
TEM	: Transmission Electron Microscopy
LPE	: Lattice Potential Energy
MA	: Mechanical Alloying
HIP	: Hot-Isostatic-Pressing
EDS	: Energy Dispersive Spectroscopy
BSE	: Back Scattered Electron

CHAPTER 1

INTRODUCTION

Light-weight materials have been commonly used in aviation, transportation, consumer electronics, biomedical devices, and alternative areas (Li & Zhang, 2019). Recently, these materials have drawn more interest due to their advantages, such as low density, high strength-to-weight ratios, and lower energy consumption (Tseng et al., 2018). Nevertheless, designing and developing new lightweight materials with high entropy alloys have become a promising approach for industrial applications (Li & Zhang, 2019).

Since the first studies about HEA systems were published, researchers have enhanced a variety of additional alloy systems that promise superior mechanical and thermal properties for specific purposes. Compared to the majority of traditional light-weight alloys, light metal containing high entropy alloys (L-HEAs) serve as new generation alloy systems because of their superior mechanical, chemical, and thermal properties.

The self-propagating high-temperature synthesis (SHS) method is an elementary, fast, and low-cost procedure used to generate metals, alloys, high-tech ceramics, and intermetallic materials (Crider,1982). The SHS method makes economical production possible by using metal oxide powders as raw materials. Furthermore, environment-friendly production is achieved with the SHS method, which requires a low energy requirement.

The production and characterization of $AlSiTiME_IME_{II}$ (ME_I, ME_{II} = Mg, Nb, V, Mn, Cr, Fe) light metal containing high entropy alloys by a SHS method is formed the aim of this thesis study. The studies are detailed in four sections: literature research, thermodynamic studies, SHS experiments, and characterization studies. In accordance with literature research and thermodynamic studies, alloy systems were determined, and SHS experiments were carried out. The obtained samples were prepared for characterization study. The microstructure and mechanical properties of L-HEAs were investigated through extensive characterization studies with scanning electron

microscopy (SEM), X-ray diffraction (XRD), X-ray fluorescence (XRF), and microhardness (micro-Vickers) test device. In future work on this Thesis study, the search for the impact of heat treatment and secondary melting process in these alloy systems is planned.

CHAPTER 2

HIGH ENTROPY ALLOYS (HEAs)

The creation and improvement of new materials has a significant impact on civilizational history. The evolution of human society and the development of materials are directly linked. The invention of new materials during each stage of human history—from the Stone Age to the Bronze Age to the Iron Age—has significantly altered human's productiveness (Li and Zhang, 2019). At the present time, a variety of materials are used in a number of different fields (Li and Zhang, 2019). The most often used materials are still the conventional alloys, such steel, aluminum, titanium, magnesium, etc. Though, these material groups could not used in some particular applications. Therefore, researchers were started alloy development for these specialized applications (Li and Zhang, 2019).

Jien-Wei Yeh and Brian Cantor independently published two papers in 2004 that introduced a brand-new alloy idea known as high entropy alloys (HEAs) (Gao et al., 2016). The HEAs are new alloy systems with superior chemical, microstructural, thermal and mechanical properties in contradistinction to conventional alloys (Miracle & Senkov, 2017). With respect to the Gibbs phase rule (Zhang, Zuo, Tang, & Gao, 2014), when the amount of the basic components in alloy increases, intermetallic compounds and complex microstructures may arise, which may contribute to brittleness and processing challenges. However, Yeh's theory of HEAs has based on alloy systems made up of at least five basic elements with concentrations ranging from 5 and 35 at. % that can be achieved without the creation of intermetallic compounds. When compared to binary or ternary alloy systems, their liquid or random solid solution possesses higher configurational entropies that can be readily created from a simple solid solution phase (Tsai & Yeh, 2014). In contrast to intermetallics repressed through solidification, solid solutions typically have superior entropy. As a result, HEAs with solid solution phases have undergone extensive research for several applications due to their promising properties.

2.1 History of HEAs

New necessities in industrial domains have resulted numerous inventions and improvements in materials science throughout time, ever since the initial alloying technique was unintentionally discovered with Cu and As in Bronze Age. Numerous studies have been taken creating novel alloy systems apart from the traditional alloys with excellent mechanical, thermal, and chemical properties in response to the rising request, particularly in the industries of aerospace and defense. Beacuse of their amazing and distinctive characteristics, including their high tensile strength, hardness values, superior oxidation and corrosion resistance, improved high-temperature mechanical capabilities, impressive thermal stability, and magnetic properties, HEA systems have received a lot of interest. After its exploration, significant research has been put into understanding the notion of HEAs. As a consequence, several sorts of HEAs has found with remarkable characteristics. HEAs are novel metallic alloys in high temperature operations in aerospace, nuclear, and chemic processes due of their attractive features. The instances of sorts of HEAs include multiphase, refractory, superalloy, lightweight, amorphous, intermetallic confined, and magnetized HEAs (Shewmon & Gill, 2018; Murty, Yeh, & Ranganathan, 2014).

The definition of high entropy alloy was first offered forth by Cantor and Yeh in 1979 and 1996, respectively. Nevertheless, Yeh and Cantor's studies about HEAs were started attention in 2004 (Murty et al., 2014). Cantor reported the equiatomic multi-principal element alloys (MPEAs) comprised of 20 elements with five atomic percentages (at.%). It is observed the creation of one main FCC phase in $Fe_{20}Co_{20}Cr_{20}Mn_{20}Ni_{20}$ (in at. %) among these alloys. In order for a single FCC structure to form, those overall systemic components are involved in a solid solution (Murty et al., 2014; Yeh, 2006). Cantor's team has conducted much research on this alloy system ever since they initial developed it. In 2004, their initial article titled "Microstructural development in equiatomic multi-component alloys" was released (Cantor, Chang, Knight, & Vincent, 2004). In 1995, Jien-Wei Yeh began investigating on HEAs and he attached credence to that high mixing entropy would affect reduction of phase number. (Gao, Yeh, Liaw, & Zhang, 2016). In order to investigate and analyze HEAs, Yeh with his assistant K. H. Huang designed fourty equivalent as-cast and

completely heat treated alloys, each with 5 to 9 elements, in 1996. The investigation demonstrated that an excellent hardness value is obtained when the quantity of constituent elements increases in the alloy systems. Besides, they did notice a slight decline in hardness value at nine-element alloy systems. In addition, they believed that those additional components and low free energy due to high configurational entropy had a great impact on resistance of corrosion.

"Nanostructured high entropy alloys with multi-principal elements - novel alloy design concepts and outcomes" namely article was published by Yeh et al in 2004 (Yeh et al., 2004). This paper became as a turning point in order for developing future generation HEAs with distinctive thermal and mechanical characteristics. Following Yeh and Cantor's pioneering studies, there has been considerable study and advancement related to HEA systems (Murty et al., 2014; Gao et al., 2016).

2.2 Thermodynamic Analysis

Entropy can be thought of as molecular randomness or disorder, simply. As the disorder of a system increases, the locations of the molecules will turn uncertain, so their entropy will increase. For example, considering the gaseous state of a substance, molecules are in random motion; they bump with one another and alter direction, so it is very tough to determine the microscopic state of the system at any given moment. Entropy is also high concerning the molecular disorder (Murty et al., 2014).

A discrete system that appears in equilibrium can contain a high level of vitality due to the constant movement of its molecules. There are many microscopic states or molecular orders in which the system can be found for each macroscopic state of equilibrium. The entropy that belongs to the system concerns the total count of microscopic states located in the system. This number is the thermodynamic probability (P), and its relationship to entropy is given by the Boltzmann relation:

$$S=k_B \ln P \qquad (2.1)$$

where k_B is the Boltzman constant (1.38 x10^{-23} J/K). Therefore, microscopically, the entropy of a system takes on a higher value when the molecular probability or randomness rises. Thus, entropy term can be identified as a measurement of molecular disorder (Murty et al., 2014).

HEAs are new alloy systems aimed at maximizing the entropy value. In HEAs, the strategy seeks to design phases of the basic structure instead of many multicomponent systems such as brittle intermetallics by decreasing the Gibbs free energy by increasing the configurational entropy ($\Delta G_{mix}=\Delta H_{mix}-T\Delta S_{mix}$). It is thought that HEAs are candidates for several potential applications since they are expected to show superior resistance to high temperature softening by enabling more effective solid solution hardening in consequence of the strong lattice defects created by the multi-alloy component (Tsai & Yeh, 2014; Murty et al., 2014).

Initially HEAs were identified as alloy systems comprised of five or more basic elements, with concentrations varying between 5% and 35% to maximize the configurational entropy and ease the creation of solid solutions (Pradeep et al., 2015). From statistical thermodynamics, the Boltzman equation helps calculate the configurational entropy of a system:

$$\Delta S_{conf} = k_B \, Inw \qquad (2.2)$$

where k_B is Boltzman constant, and w value is the number of available energy paths that particles in the system can mix or share. Table 2.1 shows the ideal configurational entropies calculated for up to nine elements for equiatomic alloys in terms of R (Yeh, 2016).

Table 2.1 Ideal configurational entropies calculated up to 9 elements for equiatomic alloys in terms of R (Yeh, 2016)

n	1	2	3	4	5	6	7	8	9
ΔS_{conf}	0	0.69	1.10	1.39	1.61	1.79	1.95	2.08	2.20

Even though the total entropy of a mixture has four types: configurational, magnetic dipole, vibrational and electronic randomness, the configurational entropy value is more effective than another types. Thus, the configurational entropy usually symbolizes a mixture's entropy to avoid complex calculations in determining another type. In Table 2.1, the configurational entropy values of the equiatomic alloys are listed in terms of the gas constant (R). It is clear that the configurational entropy rises when the quantity of elements rises (Gao et al., 2016). The entropy and the enthalpy of a mixture due to chemical bonding are the principal determinants that define the balance state when the strain energy caused by the atomic size disparity is not taken for account. Unlike negative enthalpy of a mixture (driving force for the constitutive of compounds) and positive enthalpy of a mixture (driving force to separate compounds), the entropy of the mixture is the driving force to constitute an random solid solution. Thereby, true state of balance is based on the rivalry between the relative worths of different conditions. For instance, when the creation enthalpy values of two characteristic intermetallics such as NiAl and TiAl, are divided by the points of melting belongs to those two intermetallics, 1.38R and 2.06R are obtained, respectively. It states that the driving force to form these powerful compounds occurs in this order. However, the formation enthalpy values are calculated as 12 kJ/mol for Cr-Cu and 13 kJ/mol for Fe-Cu. If the formation enthalpy values are divided by the melting temperature belonging to Cu, 1.06 R and 1.15R values are obtained, respectively. It is, therefore, logical to consider that the mixture entropy of 1.5R per mole is comparatively large to rival the enthalpy of a mixture, and a solid solution is likely to create. The ideal configurational entropy of the five-element alloy shown in the table is 1.61R. Therefore, an alloy system with at minimum five components is more likely to produce a solid solution. In most cases, random solid solutions may not occur, but solid solutions with a high rate of randomness become easy to procure. In this way, high entropy value increases reciprocal dissolubility between fundamental elements and effectually decreases the count of phases, particularly at elevated temperatures (Gao et al., 2016).

On the basis of the above explanations, there are two different ways of describing HEAs one relies on composition and another on the configurational entropy. First,

HEAs are identified as solid solution alloys, including five or more major elements. The atomic percentages of these major elements are from 5% to 35%. Their atomic ratio must be less than 5% in case of minor contributions exist. Secondly, HEAs are identified as alloys with configurational entropy values greater than 1.5R, independent of whether they consist of one or more phase at room temperature (Gao et al., 2016).

Although both definitions cover a large spectrum of alloys, they often match each other. Compounds in regions where the two definitions do not overlap are also considered HEA. Therefore, an alloy system that meets only one of these two descriptions is accepted as high entropy alloy (Gao et al., 2016; Miracle & Senkov, 2017).

From these two descriptions of HEAs, it can be understood that the fundamental principle underlying HEAs is the high configurational entropy value used to increase the creation of solid solution phases and prevent creation of intermetallic substances. This principle is crucial to avoid complex structure and embrittlement in HEA systems. The high configurational entropy also warrants that many HEAs can be appropriately produced, processed, analyzed, and utilized. Amongst the several thermodynamic factors as in the enthalpy of a mixture, configurational entropy, electronegativity, valence electron concentration, and difference in atomic radius, the name "high entropy alloy"; is suitable for MPEAs as configurational entropy is the sole determinant that rises with the incremental count of major components (Yeh, 2016).

HEAs are distinguished into three groups low entropy ($\Delta S_{conf} \geq 1.0R$), medium or moderate entropy ($1.0R \leq \Delta S_{conf} \leq 1.5R$), and high entropy ($\Delta S_{conf} \geq 1.5R$) alloys. Herein, 1.5R is accepted as the sub-limit for HEA systems. Configurational entropy values of conventional alloys are given in Table 2.2 (Yeh, 2016). In accordance with Table 2.2, low steel alloys (0.22R), Al alloys (0.43R), and Cu alloys (0.61R) have low entropy. In contrast, Ni-base superalloys (1.31R), Co-base superalloys (Stellite 6, 1.13R), 316 Stainless Steel (1.15R), and bulk metallic glasses (BMGs, $Cu_{47}Zr_{11}Ti_{34}Ni_8$, 1.17R) have moderate entropy (Yeh, 2016).

Table 2.2 Configurational entropy values of conventional alloys (Yeh, 2016)

Systems	Alloys	ΔS_{conf} at liquid state
Low-alloy steel	4340	0.22 R (low)
Stainless steel	304	0.96 R (low)
	316	1.15 R (medium)
High-speed steel	M2	0.73 R (low)
Al Alloy	2420	0.29 R (low)
Cu Alloy	7-3 brass	0.61 R (low)
Ni-based superalloy	Inconel 718	1.31 R (medium)
Co-based superalloy	Stellize 6	1.13 R (medium)
BMG	$Cu_{43}Zr_{11}Ti_{34}Ni_8$	1.17 R (medium)

2.3 Definitions of HEAs

A new category of multi-base alloys known as HEAs are random solid solutions consisted minimum 5 main components, with compositions ranging from five to thirtyfive percent atomically (Yeh et al. 2004). Additionally, the extraordinary stability of phase and mechanical characteristics of the non-equiatomic one phase $Fe_{40}Mn_{27}Ni_{26}Co_5Cr_2$ and $Fe_{37}Mn_{45}Co_9Cr_9$ HEAs were also studied by Pradeep et al. (2015). Since this investigation broadened the description of HEA systems, it is currently recognized that HEA systems can contain ratios that are non-equiatomic, nearly equiatomic, or equiatomic. In addition, HEAs may additionally include minor elements in addition to their primary constituents in order to improve the chemic, thermal, and mechanical features (Murty et al., 2014; Miracle & Senkov, 2017). As opposed to equiatomic HEAs and typical alloy systems, there are much more investigations on non-equiatomic HEAs.

With Yeh and Cantor's exploration of those novel alloys with improved mechanical, physical, and chemical properties, significant effort has been put into comprehending and improving them. FeCrMnNiCo alloy system, also known as Cantor alloy, was described by Cantor et al. (2004) as the pioneering multicomponent alloy that was composed of five transition metals. Gludovatz et al. (2014) demonstrated that Cantor alloy system with a sole FCC phase ensures superior tensile and and yield strength, when the temperature is reduced from 25 ^oC to -196 ^oC. Ti, V, Cr, Mn, Fe, Co, Ni, Cu, Nb, and Mo elements are among the metallic transition metals that comprise the

majority of HEAs. The atomic dimensions, electronegativity value, and electron valencies of all these elements are similar (Senkov & Miracle, 2001; Winter, 2020). Al is a commonly utilized metal because of the fact that it resists oxidation and wear. The probability of BCC phase creation increases with the supplement of Al to the HEAs, increasing the alloy's hardness value (Liu, Chen, Shi, Wang & Zhang, 2019; Joseph, Stanford, Hodgson & Fabijanic, 2017). Numerous investigations depend on the Cantor alloy demonstrated that the phase formation, structure, mechanical, and thermal features of HEAs are significantly impacted by the adjunct of various refractory elements and Al. In supplement to Al, refractory metals from the periodic table's transition metals like V, Mo, Ti, Ta, W, Hf, Nb, Zr, and in fact Cr are utilized to alter HEA systems. Usage these materials is purposed to develop the mechanical qualities, oxidation, and wear properties at very elevated temperatures (Senkov, Miracle, Chaput & Couzinie, 2018). Senkov et al. (2010) developed the refractory high entropy alloys, R-HEAs, with excellent mechanical properties at elevated temperature operations.

2.4 Types of HEAs

Because of their excellent tensile, chemical, and thermal characteristics when particularly in comparison to the majority of traditional alloys, HEAs are used as future generation alloys. Numerous additional alloys have been produced since the primary HEAs, which were based on transition elements, were announced, promising superior mechanical and thermal qualities for specific purposes. HEAs are classified into four categories according to their application fields. These groups consist of high entropy bulk metallic glasses (HE-BMGs), high entropy superalloys (HESAs), high entropy refractory metal alloys (R-HEAs), and high entropy light metal alloys (L-HEAs) (Murty, Yeh & Ranganathan, 2014; Gao, Yeh, Liaw & Zhang, 2014).

2.4.1 High Entropy Bulk Metallic Glasses (HE-BMGs)

Bulk metallic glasses (BMGs) and HEA systems are mathematically mixed to form HE-BMGs. In particular, HE-BMGs exhibit the characteristics of HEAs for atomic compositions that are equivalent to or nearly equal, and MGs for specimen dimensions

of a few millimeters or over. Actually, the HEA systems and BMGs' crystallographic structures are differ from one another and are constituted into a glassy and a crystalline phase, respectively. In addition, HE-BMG systems have been scientifically significantly promoted to extend the description of HEA systems from crystalline solid solutions to exact solid solutions containing only a glassy structure (Gao et al., 2014).

2.4.2 High Entropy Superalloys (HESAs)

Superalloys are alloys developed for producing aircraft turbine engines and super turbochargers that must show high performance at high temperatures (Senkov et al., 2018). These alloys are generally made by combining iron, nickel, cobalt, and chromium in different combinations. Also, low amounts of tungsten, molybdenum, tantalum, niobium, titanium, and aluminum are used. High entropy superalloys (HESAs), also known as 3d-transition-metal-based HEAs, are formed by combining the notion of HEAs and the notion of superalloys. HESAs exhibit excellent thermal stability, high oxidation resistance, and good mechanical features at high temperatures (Yang et al., 2020).

2.4.3 High Entropy Refractory Metal Alloys (R-HEAs)

Under very high temperature operating conditions, as well as ceramics, V-B group (Vanadium, Niobium, Tantalum) and VI-B group (Chromium, Molybdenum, Tungsten) metals are needed as refractory materials. Metals used as refractory materials have meager oxidation resistance, so these materials are primarily used in areas not subject to oxidation. On the other hand, Ceramic materials do not have sufficient toughness for many structural applications (Miracle & Senkov, 2017). Inadequate material technology and limitations in current technology have made using superalloy materials inevitable.

The R-HEAs are developed on 9 refractory metals with high melting points, including Mo, Nb, Ta, W, V, Hf, Zr, Ti, and Cr (Tong et al., 2005; Senkov & Miracle, 2001). Al metal is also utilized in refractory alloy systems to reduce density and increase resistance to oxidation. In the aviation sector, this quite new HEA grade is

thought to have the promise of outstanding mechanical capabilities, extreme environmental performance (resistance of corrosion and oxidation), and wear properties at even higher temperature values (Senkov et al., 2018), the nuclear industry (Detrois et al., 2019), and chemical process industry (Miracle & Senkov, 2017). It is thought that R-HEAs were developed because they outperform superalloys based on nickel in terms of high temperature mechanical characteristics.

2.4.4 High Entropy Light Metal Alloys (L-HEAs)

Light-weight materials have been commonly used in aviation, transportation (particularly electric vehicles), consumer electronics, biomedical devices, and alternative areas (Li & Zhang, 2019). Moreover, these materials have recently drawn more interest because of their advantages, such as low density, high strength-to-weight ratios, and lower energy consumption (Tseng et al., 2018). Nevertheless, designing and developing new light-weight materials with high entropy alloys has become a promising approach for industrial applications. It is thought that the L-HEAs have more excellent properties than conventional light materials in the areas of usage and properties of high entropy alloys (Li & Zhang, 2019).

Pure Ti with a density of 4.51 $g.cm^{-3}$ is utilized as a reference element, according to the definition of light materials. As we know, the densities of lithium (0.53 $g.cm^{-3}$), potassium (0.86 $g.cm^{-3}$), magnesium (1.74 $g.cm^{-3}$), beryllium (1.85 $g.cm^{-3}$), silicon (2.33 $g.cm^{-3}$), boron (2.46 $g.cm^{-3}$), aluminum (2.70 $g.cm^{-3}$) etc. metals are lower than the density of Ti element. According to the periodic table, most light-weight elements have a larger atomic radius and lower electronegativity. The difference between boiling and melting points is also greater. Hence, they are liable to have higher chemical activity. While designing the L-HEAs, these elements are not completely utilized in the novel alloys. For this reason, the progress and production of L-HEA systems are generally more difficult than conventional high entropy alloys (Li & Zhang, 2019).

Several literature studies on light metal containing high entropy alloy systems with different compositions are summarized in chronological order as follows:

Li et al. produced Mg_x $(MnAlZnCu)_{100-x}$ (x: atomic percent; x=20, 33, 43, 45.6, 50) high entropy alloys by induction melting method. Microstructure and mechanical features of $Mg_x(MnAlZnCu)_{100-x}$ alloy systems were investigated. The densities of the produced alloys are between 2.20-4.29 $g.cm^{-3}$. According to the results of the characterization studies, $Mg_{20}(MnAlZnCu)_{80}$ alloy constituted two phases: HCP and Al-Mn icosahedral quasicrystal phase. In other alloys, it was concluded that there are four phases in total: HCP, icosahedral phase, Mg, and Mg_7Zn_3. The microstructures of different alloys are relatively more complex. The hardness values of the alloys change between 178-429 HV, and the compressive strengths alter between 400-500 MPa (Li, Gao & Fan, 2010).

The melting points of $Mg_{20}(MnAlZnCu)_{80}$ and other alloys were determined as 975K and 875K, respectively, when the DSC analysis results in Figure 2.1 are examined. The peak is not observed in $Mg_{20}(MnAlZnCu)_{80}$ alloy, while a peak is observed in other alloys at 625K. It is seen that the melting point of the Mg_7Zn_3 phase is very close to 625K when the XRD and DSC results are examined together (Li et al., 2010).

The quasicrystal phase encountered in that study was found by Shechtman in 1982 (Li et al., 2010). The icosahedral phase is a phase that promotes an increase in the strength of Mg Alloys (Xu & Han, 2012). This phase also provides higher hardness value, extreme corrosion, and reasistance of heat. Al-Mn structure is an icosahedral quasicrystal phase obtained from rapid cooling (quenching) (Li et al., 2010).

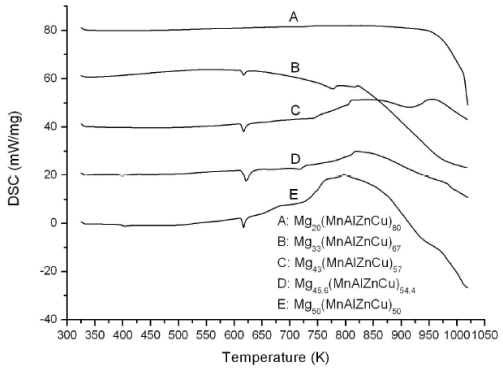

Figure 2.1 DSC curves of $Mg_x(MnAlZnCu)_{100-x}$ alloys (Li et al., 2010)

Li et al., in another study in 2011, produced MgMnAlZnCu alloy using the induction melting method. The specimens of MgMnAlZnCu alloy were annealed at 973K (700ºC) for 2 hours under an Ar atmosphere. This research examined the influences of particular cooling conditions on mechanical features and microstructure. Three different cooling conditions were used: air, water, and saltwater (Li, Gao & Fan, 2011).

When examining TEM results, it is seen that the alloy matrix consists of the HCP phase, and the pits on the matrix are in a quasicrystal structure. According to XRD and TEM results, MgMnAlZnCu alloy consists of HCP and Al-Mn quasicrystal phases. The heat stability of the Al-Mn quasicrystal structure was considerably improved with the high entropy effect (Li et al., 2011).

The lowest hardness value was obtained as 431 HV in air cooling conditions, and the highest hardness value was obtained as 467 HV in salt water cooling conditions. As a result, the hardness value increases due to solid solution hardening when the cooling rate increases. Figure 2.2 shows the results of the compressive test at room temperature. Alloys subjected to different cooling conditions have high compressive strength (428 MPa-450 MPa), while the amount of plastic deformation (3.29%-5.53%) is low. Also, the highest yield strength was obtained in salt water as 450 MPa, and the lowest yield strength was obtained as 428 MPa in air cooling conditions (Li et al., 2011).

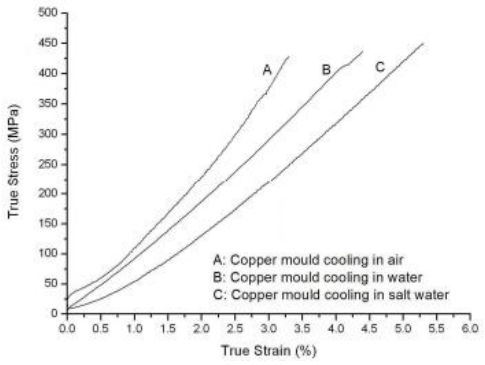

Figure 2.2 Compressive true stress-strain curves of MgMnAlZnCu alloy samples at room temperature (Li et al., 2011)

Yang et al. produced $NbTiVTaAl_x$ (x: molar ratio, x= 0-0.2-0.5-1.0) alloy systems by arc melting method, and they examined the microstructure and mechanical properties of alloy systems. According to the XRD results, all alloys have only a BCC solid solution phase. It is concluded that the admixture of Al slightly affects the phase formation of HEAs (Yang, Zhang & Liaw, 2012).

According to compressive test results, the yield strength and ductility of $NbTiVTaAl_x$ alloy systems are high. The change in yield compressive strength is that 1092 MPa, 1330 MPa, 1012 MPa, and 991 MPa, respectively, when the addition of Al is increased. Due to solid solution hardening, compressive stress increased after yield strength, and no fracture was observed under 50% compressive strain (Yang et al., 2012).

Yang et al., in another study in 2014, designed a series of low-density alloy systems containing Al, Mg, Li, Zn, Cu, and/or Sn and fabricated by the induction melting method. The designed alloy systems are as follows: AlLiMgZnSn, $AlLi_{0.5}MgZn_{0.5}Sn_{0.2}$, $AlLi_{0.5}MgZn_{0.5}Cu_{0.2}$, $AlLi_{0.5}MgCu_{0.5}Sn_{0.2}$, $Al_{80}Li_5Mg_5Zn_5Sn_5$, and $Al_{80}Li_5Mg_5Zn_5Cu_5$. According to density calculations, the lowest density value is obtained in $Al_{80}Li_5Mg_5Zn_5Sn_5$ (3.05 $g.cm^{-3}$) alloy, and the highest density value is obtained in AlLiMgZnSn (4.23 $g.cm^{-3}$) alloy. Likewise, the lowest yield strength was obtained in $Al_{80}Li_5Mg_5Zn_5Sn_5$ (415 MPa) alloy, and the highest yield strength was obtained in AlLiMgZnSn (600 MPa) alloy (Yang, Chen, Cotton & Zhang, 2014).

XRD analysis and SEM image are given in Figure 2.3. It is seen that the microstructures are commonly composed of complicated with a minimum of three components when examined in SEM images. The XRD result of AlLiMgZnSn alloy supports that it consists of more complicated structures, unlike the obtained simple microstructures from studies in the literature. It was concluded that the obtained structure consisted of Mg_2Sn and/or Li_2MgSn, α-Al, α-Zn, and α-Sn phases when the SEM micrographs and XRD results were examined together (Yang et al., 2014).

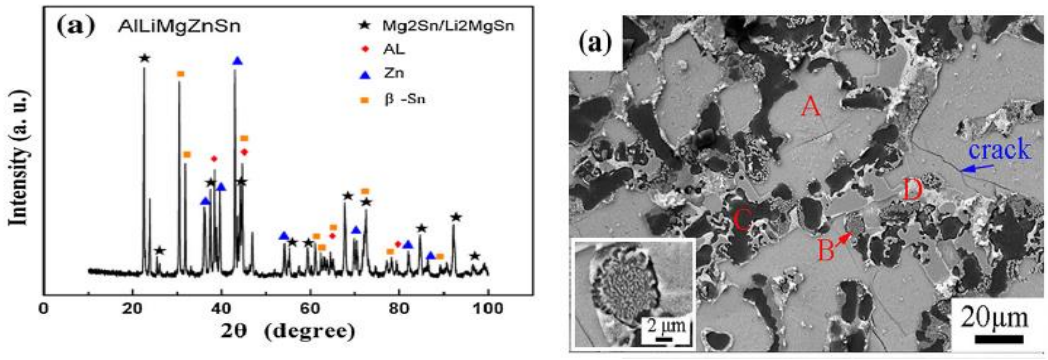

Figure 2.3 XRD analysis and SEM image of AlLiMgZnSn alloy (Yang et al., 2014)

Hammond et al., in their study in 2014, produced AlFeMgTiZn alloy by powder metallurgy method, different from vacuum arc method. The milling process was carried out at cryogenic temperatures for 10 hours. To specify their thermal stability, the milled powder mixtures were annealed at 200°C, 400°C, 600°C, and 800°C in an Ar atmosphere for 1 hour (Hammond, Atwater, Darling, Nguyen & Kecskes, 2014).

SEM images of milled AlFeMgTiZn powders treated at cryogenic temperatures for 2 and 10 hours, respectively, are given in Figure 2.4. As shown in Figure 2.4, increasing the milling time ensures a better homogeneous mixing of the elements (Hammond et al., 2014).

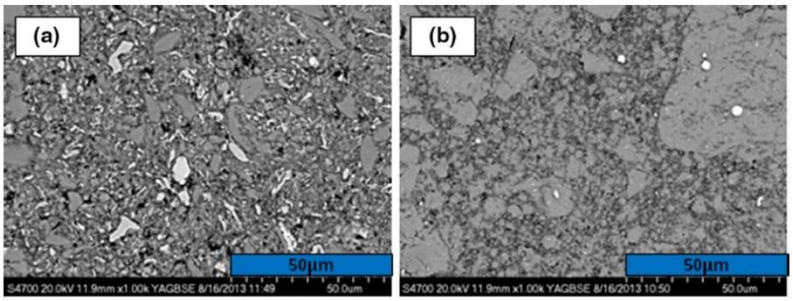

Figure 2.4 SEM/BSE images of AlFeMgTiZn alloy after milling times of a) 2 hours and b) 10 hours (Hammond et al., 2014)

According to the hardness test data, the increase in the milling time caused an increase in the hardness values. The highest hardness value was obtained at 600°C, while the lowest hardness value was reached at 800°C when the hardness test results

after the annealing process were examined. The highest hardness value before and after annealing was obtained as 800 kg/mm^2 at 600ºC (Hammond et al., 2014).

Stepanov et al. produced $Al_xNbTiVZr$ (x = 0, 0.5, 1, 1.5) alloy system by arc melting method under an Ar atmosphere. The produced alloys were annealed at 1200°C for 24 hours. The structural and mechanical features of the HEAs after as-cast and annealing were investigated (Stepanov, Yurchenko, Shaysultanov, Salishchev & Tikhonovsky, 2015).

As shown in the XRD results (Figure 2.5), all alloy systems consist of two phases: the Laves phase and BCC structure. The Laves phase has a hexagonal C14 structure. In AlNbTiVZr HEA, the dominant phase is consisted of the BCC structure, and the Laves structure is also seen as small peaks. When the Al amount in the alloy increases, the peak intensity of the BCC phase decreases. In contrast, the peak intensity of the Laves phase increases gradually. According to the XRD results after homogenization annealing, NbTiZrV alloy is composed mainly of BCC structure and trace of Laves phase. It is seen that the peak intensity of Laves phase increased while the BCC phase remained the same when compared with the obtained analysis results before and after annealing of $Al_{0,5}NbTiVZr$ alloy. Moreover, the Zr_2Al phase with hexagonal structure emerges. The increment in Al content in AlNbTiVZr and $Al_{1,5}NbTiVZr$ HEAs causes a drop in the peak density of the BCC structure while incrementing the peak intensity of Laves and Zr_2Al phases. Furthermore, the increment in the quantity of Al in these $Al_xNbTiVZr$ alloy system effects to reduction in the intensity from 6.49 g.cm^{-3} to 5.55 g.cm^{-3} (Stepanov et al., 2015).

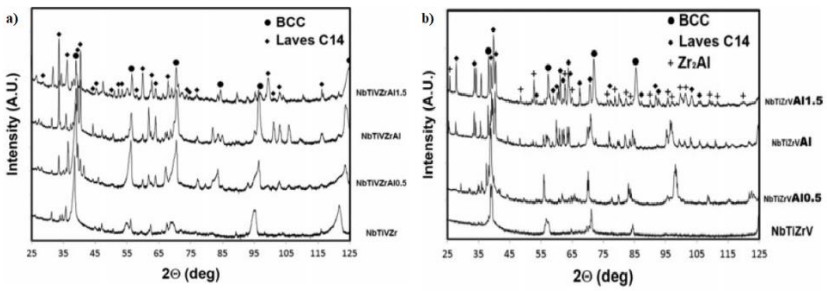

Figure 2.5 XRD analysis of $Al_xNbTiVZr$ (x = 0-0.5-1-1.5) alloys after a) as-cast, b) after annealing (Stepanov et al., 2015)

It is observed that the microhardness values of HEAs rise with the increment in the amount of Al when the mechanical properties of the alloys are examined. For instance, the lowest hardness value (380 HV) is seen in NbTiVZr alloy, and the highest hardness value (620 HV) is seen in $Al_{1.5}$NbTiVZr alloy. According to the hardness test data after heat treatment, it is concluded that the annealing process does not significantly impress the hardness values of other alloys apart from NbTiVZr. Concerning the compression test results, the lowest yield strength is obtained in $Al_{0.5}$NbTiVZr alloy (960 MPa), and the highest yield strength is obtained in NbTiVZr alloy (1320 MPa) (Stepanov et al., 2015).

In another study by Stepanov et al. (2015), $AlCr_xNbTiV$ (x = 0, 0.5, 1, 1.5) alloy systems were generated by the arc melting method. As in previous research, the produced alloys were annealed at 1200ºC for 24 hours. After the annealing process, HEAs' microstructure and mechanical properties were investigated at different temperatures (at 22ºC - 1000ºC) (Stepanov, Yurchenko, Skibin, Tikhonovsky & Salishchev, 2015).

It was observed that AlNbTiV HEA had the lowest density value as 5.59 $g.cm^{-3}$. According to compressive test data, all alloy systems reach the highest yield strength value at 22ºC. The highest yield strength was achieved in the $AlCr_{1.5}$NbTiV HEA system (1700 MPa). The compressive strength of the HEAs rises at between 22ºC to 800ºC temperatures as the addition of Cr increases. Furthermore, it was seen that the ductility increases as the temperature increase when the stress-strain curves of the alloys (Figure 2.6) are examined. It was concluded that it has higher specific yield strength in the temperature range of 22ºC-800ºC when $AlCr_{1.5}$NbTiV alloy is compared with CrNbTiVZr, Inconel 718, and γ-titanium aluminide-based TNM alloys (Stepanov et al., 2015).

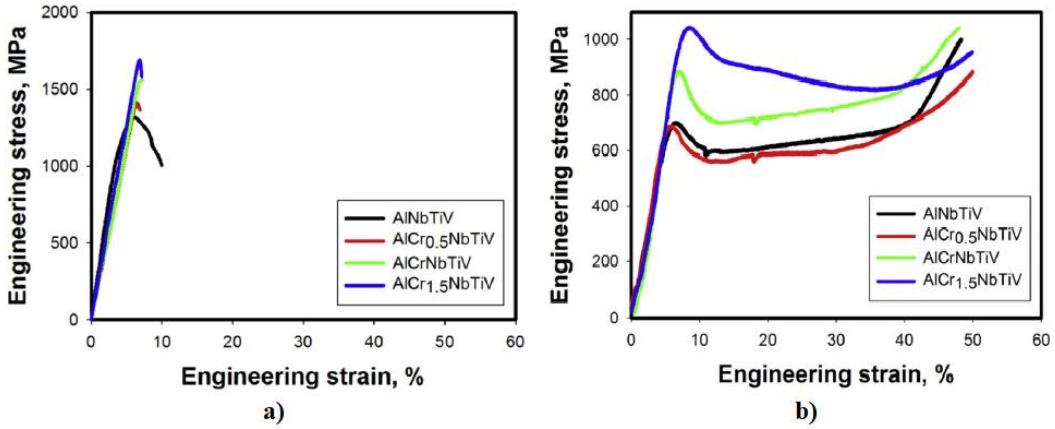

Figure 2.6 Compressive stress-strain curves of $AlCr_xNbTiV$ (x = 0-0.5-1-1.5) alloys a) at room temperature, b) at 800°C (Stepanov et al., 2015)

2.5 Four Core Effects

The structure and essential characteristics of HEA systems are determined by a number of major characteristics. The essential characteristics are related to the physical metallurgy of HEAs. HEAs' physical metallurgy is studied under "four core effects" headings: high entropy, sluggish diffusion, lattice distortion, and cocktail effect (Yeh, 2013).

The high entropy effect is critical for the thermodynamic approach to provide basic solid solution phases by HCP, BCC, or FCC phases. In addition to the deformation concept and each of the interactions among each characteristic in structure and microstructure are influenced by this effect (Gao et al., 2016). Sluggish diffusion effect is related to phase transition kinetics. The cocktail effect, that gives the composite influence upon characteristics as a result of the interaction in both the dissimilar atoms, is the final effect. Below is a detailed explanation of these consequences (Yeh, 2013).

2.5.1 High Entropy Effect

The effect of high entropy is a binding effect in order for HEA systems to form basic solid solution phases and enhance the microstructure relative to how it is

previously predicted. The total count of expected phases is influenced by a variety of factors, in accordance with the Gibbs phase rule (Zhang et al. 2014). These are the system's freedom degrees (F), phase counts (P), and component counts (C), all calculated under equilibrium conditions and stationary pressure. These are the freedom degrees (F) in a system, counts of the phases (P), and counts of components (C) at constant pressure in equilibrium conditions. According to this formula, the concentrated system's balance state and total phase quantities cannot exceed C+1. In dissimilar circumstances such as F value is 0, the phase quantities may decline.

$$P+F=C+1 \tag{2.3}$$

Owing to its superior configurational entropy values, the number of phases acquired from HEAs deviates from the highest number of phases specified by the Gibbs phase rule. Let us suppose that the dissolvability of these phases inside itself is made simpler by the high entropy. As a result, that effect eliminates creation of numerous undesired phases. The emergence of several phases in such HEAs is kinetically constrained due to the low of atoms diffusion ratio. Consequently, in HEAs, nominal diffusion ratio and superior configurational entropy value have a considerable affect on the phase counts (Murty, Yeh, Ranganathan & Bhattacharjee, 2019).

Table 2.3 is shown mixture enthalpy (ΔH_{mix}), mixture entropy (ΔS_{mix}), and mixture Gibbs free energy (ΔG_{mix}) values of the basic and intermediary phases, composites, and spontaneous solid solutions with n-element HEA systems comparatively. These thermodynamical values of basic phases have nearly 0 since they just include a major metal. ΔS_{mix} is nearly 0 owing to low mixture entropy value in regular structures. In addition to this, other important thermodynamical values of composite phases largely lower than 0. On the contrary, in spontaneous solid solutions referred to as HEAs, mixture entropy and mixture enthalpy are greatest and moderately negative, respectively (Yeh, 2013).

Table 2.3 n-element HEA systems with strong interelement connections: ΔH_{mix}, ΔS_{mix}, and ΔG_{mix} values of the basic and intermediary phases, composites, and spontaneous solid solutions (Yeh, 2013)

Comparative States	Elemental Phases	Compounds	Intermediate Phases	Random Solid Solutions
ΔH_{mix}	~0	Large negative	Less large negative	Medium negative
ΔS_{mix}	~0	~0	Medium	$\Delta S_{\text{mix}} = -R\sum_{i=1}^{n} X_i \ln X_i$
ΔG_{mix}	~0	Large negative	Larger negative	Larger negative

There are many researches in the literature that provide proof of the high entropy effect (Tsai & Yeh, 2014; Del Grosso, Bozzolo & Mosca, 2012). In order to demonstrate this effect Figure 2.7 displays the relative grades of the mixture free energy curves of a random solution, pure elements, intermetallic composites (AB) at 1473 K (1200ºC) for equivalent HEA system comprising 8 components. At 1200ºC, -23 kJ/mol is assumed to represent the mean mixture energy among 2 atom combinations (Takeuchi & Inoue, 2000). We can infer that the alloys with 8 components have the minimum free energy. This provides crucial proof that HEAs are thermodynamically steady.

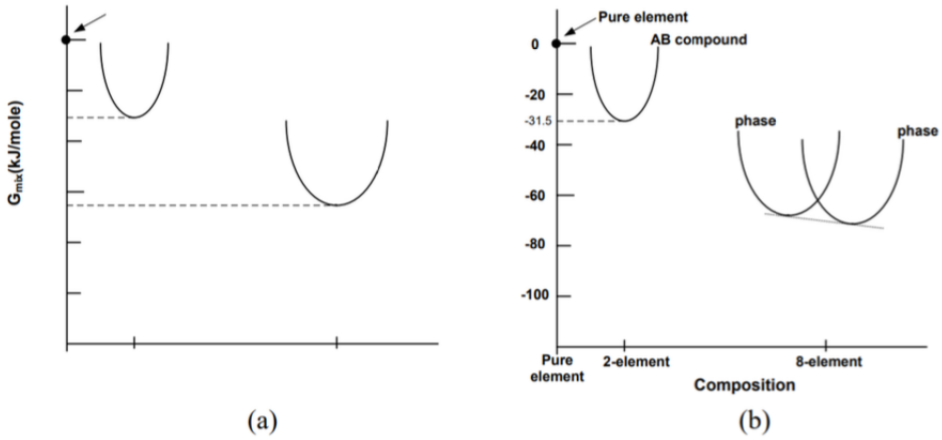

Figure 2.7 A comparison of the mixed free energy curves for three different states, namely a random solution, a pure element, and a composite at 1473 K (1200ºC) for an equivalent HEA comprising 8 elements for one steady phase, (a), and for 2 concurrent phases, (b). (Takeuchi & Inoue, 2000)

2.5.2 Lattice Distortion Effect

Due to the difference in atomic radius across elements, structural stress and strain result from another element being wholly dissolved in a matrix and having other distinct atoms surround it. The variances of dissimilar binding energies among the basic metals and the crystal structure among the basic metals also induce a rise in lattice distortion (Senkov et al., 2010; Ng, Guo, Luan, Shi & Liu, 2012).

According to a research by Senkov et al, equivalent HEA alloy system based on FeCoCrNiMn possesses one FCC phase with 1192 MPa Vickers hardness under homogeneous circumstances, compared to 864 MPa computed by the admixture principle. Additionally, the 5250 MPa hardness value of the equivalent refractory HEA sytem based on MoNbTaVW has been more than 3 times better than of 1596 MPa achieved via the principle of admixture and it contains a BCC crystal structure. It is commonly known that alloys consisting of BCC exhibit substantially higher solid solution hardening than alloys consisting of FCC (Senkov et al., 2010).

2.5.3 Sluggish Diffusion Effect

On account of reach the compositional partitioning in HEA systems, the creation of novel phases needs the co-diffusion of several distinct sorts of atoms. HEA systems may contain either spontaneous or regular sorts of solid solutions, as indicated in the heading above. The HEAs' matrices can indeed be regarded of as totally solvable. As a consequence, an atom's diffusion behavior in a totally dissolving matrix would differ from an atom's diffusion behavior in the matrix of traditional alloy systems. During diffusion, atoms of different elements encompass an emptiness in the matrix. It is asserted that HEA sytems own larger activation energies that are deeply relevant to sluggish diffusion kinetics because the lattice potential energy (LPE) within lattice regions has shifted dramatically. Atomic diffusion in the network would be hampered by the nominal LPE regions. This effect is a result of the current situation (Tsai, Tsai & Yeh, 2013).

The nucleation, growth, distribution, and morphology of the created phases are all expected to have direct impacted by sluggish diffusion. In essence, by modifying the material's microstructure, it enhances the material's qualities. For instance, it is easily got ultrafine precipitates within HEA systems (Liu, Wu, He, Nieh & Lu, 2013). As an outcome, the alloy's recrystallization temperature is rising and the ratios of grain growth and particles coarsening decline. Thus, enhanced creep resistance can improve the useful life of components utilized at elevated heats.

2.5.4 Cocktail Effect

According to the "cocktail effect," HEAs may exhibit surprising characteristics when more than 5 fundamental components exist. The concept for cocktail effect was primary put up by Ranganathan in a publication called "Alloyed pleasures: multimetallic drinks." (Ranganathan, 2003).

Because the number of phases in HEAs can vary with composition, each of the phases that make it up a HEA influence overall distribution, size, and other physical characteristics. Essentially, those alloys' characteristics closely resemble those of composites made up of a minimum of two components with radically dissimilar chemical or physical features. To put it another way, every phase could also be thought of as an attribute of the composite material. According to the admixture principle, composites characteristics are a synthesis of the individual features of the fundamental elements as well as inherent connections with one another and the lattice distortion effect. More critical than the admixture principle is how the metals interact with one another and the lattice distortion effect. There are numerous researches in the literature that illustrate how this feature affects various HEA sytems (Arons, 1992; Gaskel, 2003; Tong et al., 2005).

Figure 2.8 provides a clearer illustration of the cocktail effect by demonstrating how the hardness value of $Al_xCoCrCuFeNi$ alloy systems alters as a proportion to the Al quantity (Yeh, 2006). This illustrates that the hardness value belonging to these HEAs is considerably improved when Al concentration in HEA is promotedMoreover, the phase transition between FCC through BCC is seen as an outcome of the rise in Al

quantity. Those effect that the interaction of the constitutive factors describes is strongly correlated to this. To put it another way, the strong interplay connection between Al and other components causes the formation of a tough BCC phases when the Al proportion of HEAs is enhanced.

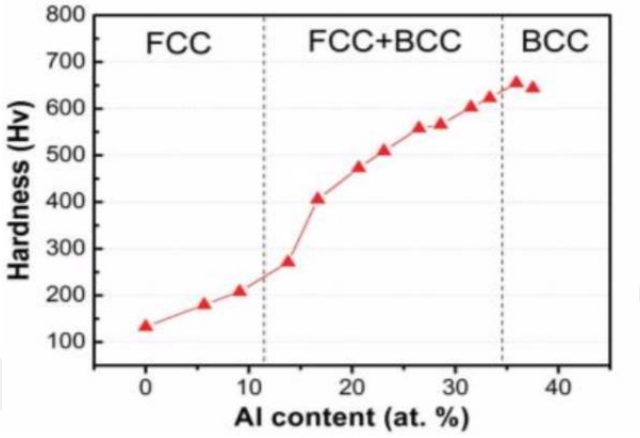

Figure 2.8 $Al_xCoCrCuFeNi$ alloys' variation in hardness value in relation to the amount of Al (Yeh, 2006)

CHAPTER 3

HEAS' MANUFACTURING TECHNIQUES

3.1 Manufacturing from the Liquid Condition

Foremost popular procedure to generate the alloy system from a liquid metal are arc furnaces and induction furnaces. Nevertheless, these two sorts of melting procedures have different process principles. The operation of melted raw materials by creating an arc among a charged material and an electrode material is termed as the arc melting procedure. The induction melting procedure, besides, is associated with the production of an eddy current in the element (often has conductive metal), thereby raises the metal's heat to its melting point. For metals with nominal melting points, namely Mn, Zn, and Mn, the induction furnace procedure is considerably extra appropriate than the other procedure.

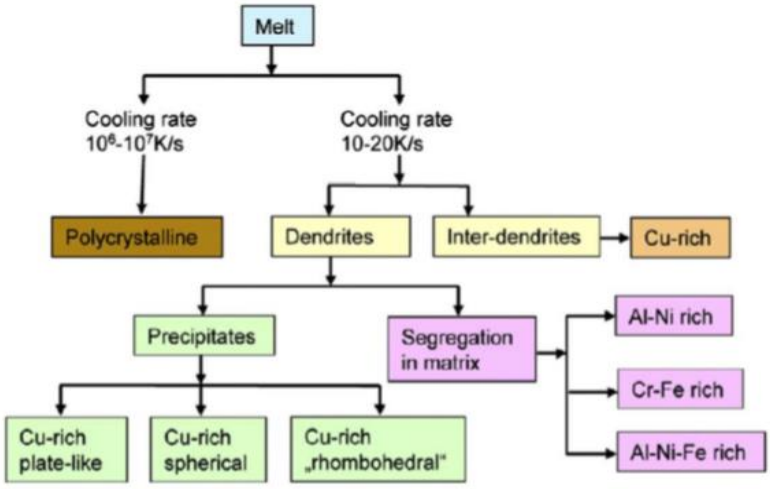

Figure 3.1 Graphical view of phase separation throughout the solidification of AlCoCrCuFeNi HEA system by the splat quenching technique and casting process (Singh et al., 2011)

Singh et al. (Singh, Wanderka, Murty, Glatzel & Banhart, 2011) produced AlCoCrCuFeNi HEA system by casting process and subjected it to a splat quenching process. The cooling rate in the casting process was determined as 10-20 Ks^{-1}, while in the splat quenching process, the cooling rate was chosen as 10^6 -10^7 Ks^{-1}. Figure 3.1

describes the phase separation of HEA throughout splat quenching and solidification by casting. The microstructural changes in the HEAs according to cooling rate were studied. That investigation is reported elemental seperation under nominal cooling rates is the major reason of dendritic microstructures that are seen. This creation of nanometer-sized polycrystalline structures, moreover, originates from rapid cooler (Singh et al., 2011).

3.2 Manufacturing from the Solid Condition

Mechanical alloying (MA) is the approach of solid condition synthesis that is widely frequently applied. That approach could be summarized as just an operation that entails repeatedly cold welding the materials and fractured them with an elevated energy ball mill, afterward re-welding those (Suryanarayana, 2001). In these days, the MA approach is frequently utilised combine elemental microparticles to create alloy systems in both balance and nonequilibrium status. There are three major steps in the MA procedure. Initially, ball milling is used to grind raw material into finer particles. The next step is the hot-isostatic-pressing (HIP) procedure, which involves concurrently compressing and sintering particles. In order to eliminate inner tensions created throughout the alloying operation, a heat treatment is given finally (Suryanarayana, 2001).

3.3 Manufacturing from the Gas Condition

HEA systems are commonly created using the protective coatings technique called as sputter deposition. That technology can also be characterized as a 2^{nd} ion bombardment-based layer creating operation on the material surface. HEA coatings have been deposited on $(AlCrTaTiZr)N_x$ alloy by the sputtering deposition technique towards tribological purposes by Chang et al. (Chang, Lin, Huang & Wu, 2010). On the mechanical characteristics, creep conduct, interface adhesion, and deformation mechanisms of coverings, the impact of the alteration in N quantities was analyzed. The results of the mechanical characterization indicated that the coated surfaces' hardness rose significantly between 13 GPa towards 30 GPa (Chang et al., 2010).

CHAPTER 4

SELF-PROPAGATING HIGH-TEMPERATURE SYNTHESIS (SHS)

The self-propagating high-temperature synthesis method was discovered in Soviet Union. It is an elementary, fast, low-cost procedure used to generate metals, alloys, high-tech ceramics, and intermetallic materials (Crider,1982). Furthermore, the SHS method makes economical production possible by using metal oxide powders as raw materials. Environment-friendly production is achieved with the SHS method, which requires low energy (Alkan, 2014).

The operation of the process is that the excessive exothermic reaction commences automatically by triggering and progresses over the reaction mix in the figure of a wave. Therefore, for the reaction to proceed spontaneously, the reaction must possess comparatively great activation energy and produce extremely high heat. The SHS process is characterized by many properties that can be individuated from traditional generation procedures. Advantages; high heat, excellent reaction speed (0.15 m/s), which allows the generation of materials at temperatures 800-4500°C without utilizing an external heat resource, higher purity as it evaporates impurities with low boiling temperatures due to high temperatures, simple exothermic reaction. It can be counted as no need for expensive investment and equipment (Merzhanov, 2002).

4.1 History of SHS

Although Beketov discovered the metallothermic reaction in 1865 and Goldschmidt in 1895, the discovery of the solid flame and the formation of SHS by Merzhanov et al. in 1967 (Merzhanov, 2012). Although it is theoretically known that metal can be produced by reducing oxides with aluminum, metal production could not be done in this way because the reaction was not fully controlled. The first successful study on this subject was made by Frederik C. Weber in 1902. In this study, metal oxides and aluminum wires were taken into a crucible. It was determined that the

reaction was successful when sufficient heat was applied due to dehumidifying the charge.

Clarence F. Hislrey, Brooklyn, and Jean A. Lamoureux carried out the first study in which metal oxide was reduced, and metal formation was achieved by a metallothermic process in 1959. This study aims to separate metal and slag by designing a crucible under conditions where the reaction can start and continue. The metal oxide-reducer mixture was subjected to preheating, after which heat was added to the mix to trigger an exothermic reaction. The active ingredient in the charge has been replaced by the less active one. In the study, Fe_3O_4 was reduced with Al, and the reaction took place as follows (Hislrey & Jean, 1956):

$$3Fe_3O_4 + 8Al \rightarrow 9Fe + 4Al_2O_3 + heat \qquad (4.1)$$

Aluminum, which is more active in this reaction, was combined with oxygen, and iron was obtained from iron-oxide. As a result of the reaction, metal and slag were separated from each other. The reaction took place in approximately 20 seconds, and it was determined that a temperature of 2500 ^oC was reached (Hislrey & Jean, 1956).

The first study on homogeneous thermal explosion and ignition processes in dense phases, both theoretically and experimentally, was conducted in 1967 by A.G. Merzhanov and his working group (Merzhanov, 1967).

Various inorganic compounds such as carbide and boride of the metals in the 6th group have been produced. At least one of the metals such as Ti, Zr, or Hf is mixed with a non-metal component such as N_2, C, B, Si, O_2, P, S, F, or Cl_2, the generation of a sufficient temperature for the start of the combustion process is achieved by ignition and the with the advancement of this heat wave, the production of refractory inorganic compounds under a protective atmosphere has been completed (Merzhanov, Shkiro & Borovinslaya, 1975). The production of intermetallic compounds by combustion synthesis dates back to the 1970s (Varna & Mukasyan, 2002).

4.2 Termodynamics of SHS

Many experimental investigations are conducted to figure out the mechanism of the SHS technique. In this direction, various experimental methods and theoretical definitions have been developed.

The most basic reactions of SHS synthesis are listed below (Merzhanov, 2002). Synthesizing from the elements:

$$Ni + Al = NiAl \quad (4.2)$$

$$3Si + 2N_2 = Si_3N_4 \quad (4.3)$$

Metal oxidation by metal oxide mixtures:

$$3Cu + 2BaO_2 + 1/2Y_2O_3 + 0.5(1.5 - x)\ O_2 = YBa_2Cu_3O_{7-x} \quad (4.4)$$

Synthesis from compounds:

$$PbO + WO_3 = PbWO_4 \quad (4.5)$$

Thermal degradation:

$$2BH_3N_2H_4 = 2BN + N_2 + 7H_2 \quad (4.6)$$

In the SHS method, after the initial mixture is given a small amount of initial heat to bring the mixture to the ignition heat, the reaction progresses automatically without the requirement for exterior energy. The heat emerges in every layer, moving towards the following unreacted mixture layer. In other words, this heat forms the initial heat for that layer to ignite and increases the temperature. At the same time, the front side of the SHS reaction surpasses the combustion products back; it moves towards the unreacted mix and separates the heat-affected zone and the reaction zone. The high amount of heat energy generated during the application directly impresses reaction speed, providing a very economical and highly productive generation possibility by incremental speed (Munir & Tamburini, 1989).

In the SHS method, many different techniques are used as an igniter to initiate reactions. Generally, W wire, which can reach the required temperature in order to start the reaction with electricity, is used by dipping into the powders. If necessary, powders of various compounds are added to the starting mixture. A laser or microwave is also used to initiate the SHS reaction. It is possible to achieve a very high heat flow density utilizing a laser. In addition, the reaction can be performed by heating the starting mixture to ensure the continuity of the SHS reaction (Mossino, 2004).

In SHS reactions, the combustion temperature is connected to the difference in enthalpy between reactants and products. These critical temperatures are (Biswas, Roy, Gurumurthy, Prabhu & Banerjee, 2002):

- **Initial temperature (T_0):** It refers to the starting powder's temperature before the reaction.
- **Ignition temperature (T_{ig}):** The specific starting temperature varies depending on the kinetic characteristics of the reaction.
- **Adiabatic temperature (T_{ad}):** Underneath adiabatic circumstances, the greatest temperature can be achieved. This temperature is connected to the exothermic state and the starting temperature.
- **Actual combustion temperature (T_c):** The maximum temperature can be achieved underneath nonadiabatic states. It can be controlled kinetically related to the heat lost occurring during the reaction.

During SHS experiments, T_o, T_{ig}, and T_c temperatures are measured empirically. The T_{ad} temperature can be thermodynamically calculated using the initial temperature. For SHS reactions to occur, the T_{ad} value must be 1527^{o}C (Munir & Tamburini, 1989).

CHAPTER 5

EXPERIMENTAL PROCEDURE

The light metal containing high entropy alloy systems was selected as $AlSiTiME_IME_{II}$ (ME_I, ME_{II} = Mg, Nb, V, Mn, Cr, Fe). The SHS method was chosen when producing light metal containing high entropy alloys. Project studies have been collected under three main headings: thermodynamic studies, SHS experiments, and characterization studies. The flow-process diagram of studies is given in Figure 5.1.

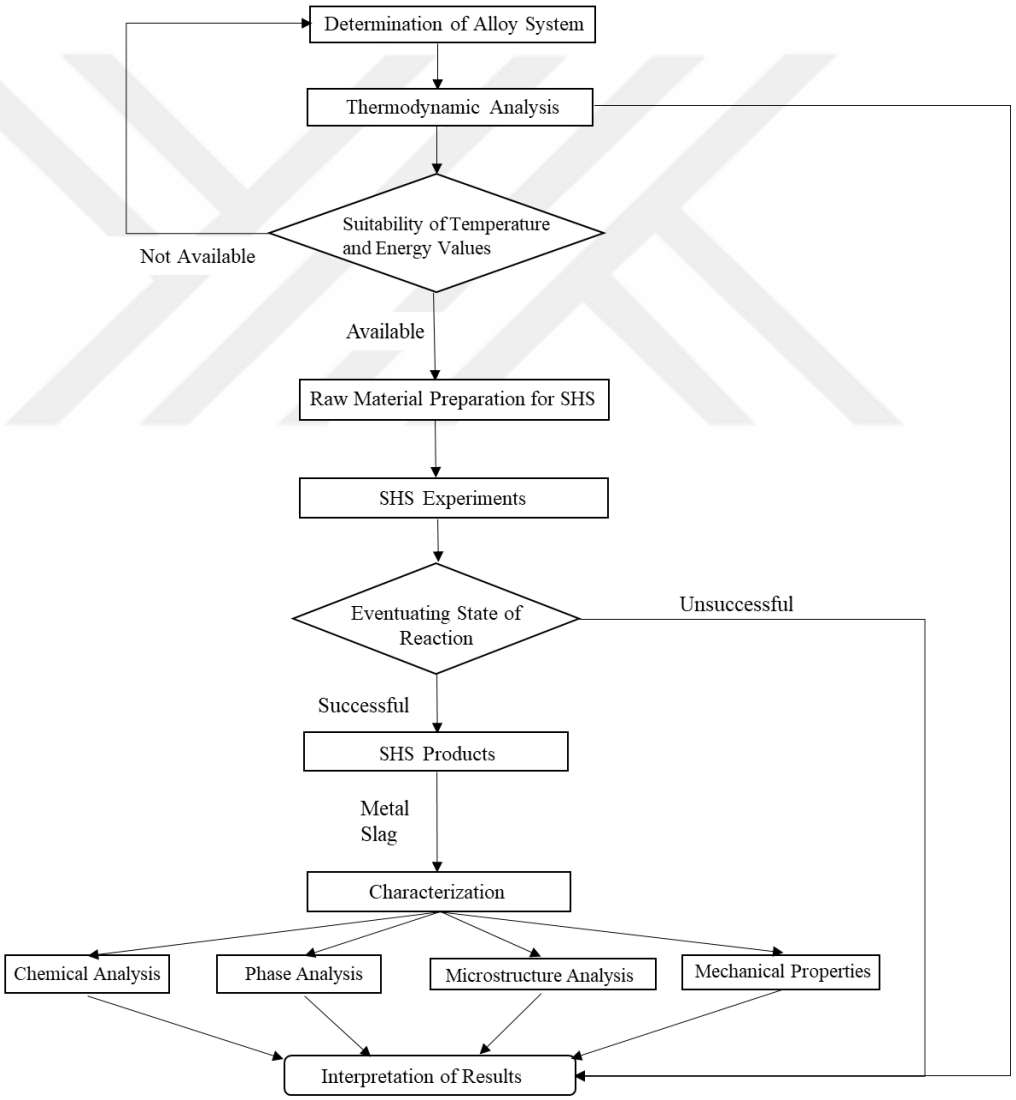

Figure 5.1 Flow-process diagram of experimental studies

This study chose light metal containing HEAs as the target alloy system. Various metal oxide powders and reductant metal powder mixtures were used in SHS experiments during the production of alloy systems in accordance with thermodynamic studies.

5.1 Materials

In SHS experiments, various metal oxide powders and different reductant metal powders (Al, Mg, and Si) were provided in different physical properties and purities to produce the specified target alloy systems. Two conditions were sought, namely particle size and purity, for the raw materials. The metal oxide powders' average particle sizes were 75 - 150 µm, and their purity was at least 98%. The metal oxide powder mixtures were composed of TiO_2, V_2O_5, Nb_2O_5, MnO_2, Cr_2O_3, CrO_3, and Fe_2O_3, while the pure raw materials were composed of metallic Al, Mg, and Si powders. Metallic Aluminum metal powders were obtained from Çukurova Kimya Endüstrisi A.Ş, and metallic Si metal powders were obtained from AVEKS. The purity of metal powders is at least 98%, and the average particle size is below 250 µm.

5.2 Methods

5.2.1 Thermodynamic Analysis

Thermodynamic analyses of the selected alloy systems were made using HSC Chemistry 6.2 software and Thermo-Calc software with related databases. During the examinations, the "Reaction Equations" and "Heat and Material Balances" modules within the HSC Chemistry 6.2 software and the "One Axis Equilibrium" template of Thermo-Calc software were used. Using these modules, the free energy, enthalpy, adiabatic temperature, and specific heat (J/g) values of the reactions were calculated. In addition, the phase changes that occur in the structure of a system, given the initial conditions (the elements contained in the alloy, element compositions, temperature, pressure, etc.), during regular cooling, the temperatures at which these changes occur, the ratios and compositions of the formed phases were also calculated. Standard free energy change ($\Delta G°$), standard enthalpy change ($H°$), standard entropy change ($\Delta S°$), specific heat (C_p), and solution constant (K_{eq}) values of reactions are calculated under different temperature and pressure values. These values were figured out thanks to the

"Reaction" module. Thermocalc software was used to support the characterization steps of the obtained alloys as a result of SHS experiments. The chemical compositions of the obtained SHS alloys were chosen as the initial conditions of Thermo-Calc calculations.

5.2.2 SHS Experiments

The equiatomic $AlSiTiME_IME_{II}$ (ME_I, ME_{II} = Mg, Nb, V, Mn, Cr, Fe) light metal containing high entropy alloys were produced by a self-propagating high-temperature synthesis starting from metal oxide powder mixtures. Alloys were chosen to have appropriate specific heat and adiabatic temperature for SHS reactions, and the experimental studies were carried out. In addition, the number of main elements was selected as 5, 6, and 7 in L-HEA system, and the experiments were carried through. The starting metal oxide and reductant amounts were calculated for the equiatomic L-HEA alloy system, and the raw material powder mixtures were prepared for production. The basic chemical reactions of L-HEAs that are atomically equivalent or equimolar to each other during SHS production are given below:

$$TiO_2 + ME_IO + ME_{II}O + v_1\,Al + v_2\,Si + v_3\,Mg = AlSiTiME_IME_{II} + y_1\,Al_2O_3 + y_2\,SiO_2 + y_3\,MgO \quad (5.1)$$

SHS experiments were carried out under atmospheric conditions, and no protective gas was supplied to the system. Metal oxide powders to be used as raw materials were kept in the drying oven at 105°C for at least 2 hours to remove the moisture. The raw material powder mixtures were calculated according to the target alloy composition and were weighed on a precision scale to have a total weight of 150 g. The mixture was placed in a plastic box and mixed in an Emor brand powder mixer at 600 rpm for 15 minutes. After the mixing process, the raw material powder mixture was fed into the copper crucible. The design of the crucible consists of a base and a cylindrical part that fit into each other. The lower part is 70 mm in diameter, while the cylinder part consists of 200 mm height, 70 mm outer, and 60 mm inner diameter. 0.80 mm diameter Cr25Al5 wire was placed on the surface of the raw material powder mixture in the Cu crucible, and the crucible was covered with a lid. SHS reactions were initiated by giving power over the resistance wire at a maximum of 40 volts and 30 amperes and triggering an increase in the temperature of the resistance wire. The crucible was

cooled rapidly in water, and metal and slag were obtained (Figure 5.2) after the SHS reactions were completed.

Figure 5.2 The images of obtained product as a result of SHS experiments

The alloys and slags were stored separately for characterization processes after weighing. The schematic view of the SHS Experiments and the progression of the combustion wave in the SHS experiment is given in Figure 5.3(a, b).

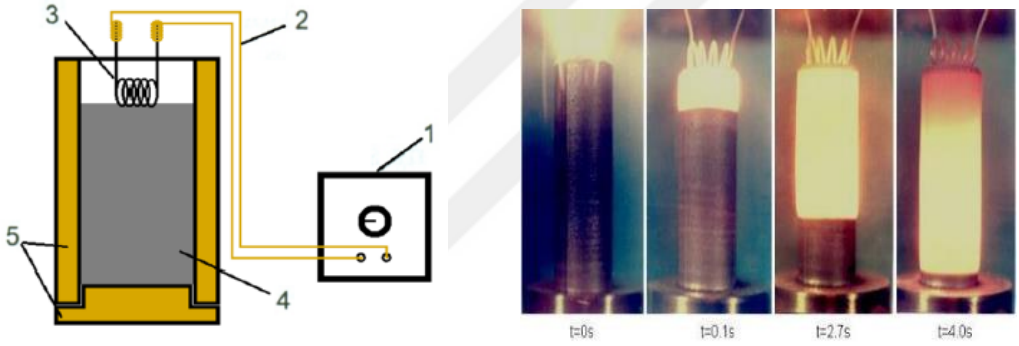

Figure 5.3 a) The schematic views of SHS experimental setup, (1) power supply, (2) Cu connecting cable, (3) igniter, (4) starting raw material mixture, (5) Cu crucible, and b) the progressing of the combustion wave in SHS experiment (Alkan, 2014; Merzhanov 1995)

5.2.3 Characterizations

The raw materials, the by-products, and final products in the experiments were identified by various characterizations. These included chemical, phase, microstructure, and mechanical tests. Chemical analyzes were performed using the X-ray fluorescence (XRF) technique. X-ray diffractometers (XRD) device was utilized for the phase analyzes. JEOL JSM-6060 SEM Device was used for microstructure images, while IXRF SYSTEMS Inc Device was used. For microstructure analysis, grinding of metallurgical samples was performed with 80, 240, 400, 800, and 1200 grit abrasive papers, respectively, in the sample preparation laboratory, and then the

polishing proceeded. The grinding and polishing process was carried out with the PRESI MECAPOL P 230 Grinding - Polishing device. In the polishing process, 3-micron water-based single crystal diamond paste supplied by Metkon company was used. Shimadzu HMV-2 microhardness (micro-Vickers) device was used to analyze mechanical properties. Five Vickers hardness values were recorded by applying a 0.3 kg load to the samples. These values were averaged and calculated as standard deviation values.

CHAPTER 6

RESULTS AND DISCUSSIONS

This section gives thermodynamic examinations, SHS reactions, and characterization results mainly.

6.1 Thermodynamic Results and Discussion

Metallothermic reduction of a metal compound occurs when the metal used as the reductant has a higher affinity for the metal to be reduced than the non-metal compound. For example, aluminum is a metal having a high affinity for oxygen. As the difference in the oxygen affinities between Al and the targeted metal increases, reducing this metal oxide with Al becomes easier. The affinity of metals for oxygen is related to the ΔH value, which is the formation energy of their compounds. The formation enthalpy values of some metal oxides per mole of oxygen are given in Table 6.1.

Table 6.1 Formation energies of metal oxides (Hall, 2012)

Formation reaction of metal oxide	**The formation energy of the reaction ($\Delta H°_{298}$)**
$4/5\ Nb + O_2 = 2/5\ Nb_2O_5$	– 760 kJ/mol O_2
$4/5\ V + O_2 = 2/5\ V_2O_5$	– 617 kJ/mol O_2
$Ti + O_2 = TiO_2$	– 944 kJ/mol O_2
$4/3\ Fe + O_2 = 2/3\ Fe_2O_3$	– 547 kJ/mol O_2
$Si + O_2 = SiO_2$	– 910 kJ/mol O_2
$2Mg + O_2 = 2MgO$	– 1.202 kJ/mol O_2
$4/3\ Al + O_2 = 2/3\ Al_2O_3$	– 1.118 kJ/mol O_2
$2/3\ Cr + O_2 = 2/3\ CrO_3$	– 387 kJ/mol O_2
$4/3\ Cr + O_2 = 2/3\ Cr_2O_3$	– 748 kJ/mol O_2
$Mn + O_2 = MnO_2$	– 517 kJ/mol O_2

The Gibbs Standard Free Energy value indicates the stability of a metal oxide. A negative Gibbs Standard Free Energy value means the reaction will occur spontaneously. The more negative values in the change of free energy specify an increase in the tendency of the reaction to occur. The metal oxide with more negative values has higher stability at the specified temperature. The Gibbs free energy changes of metal oxides at varying temperatures under one mole of oxygen gas are shown in the Ellingham diagram (Figure 6.1) (Alkan, 2014).

The stability of the oxides increases, the affinity increases, and the Gibbs standard free energy value decreases when moving down the Ellingham diagram. The temperature increases, affinity decreases, stability of oxides decreases, and entropy increases when moving from left to right.

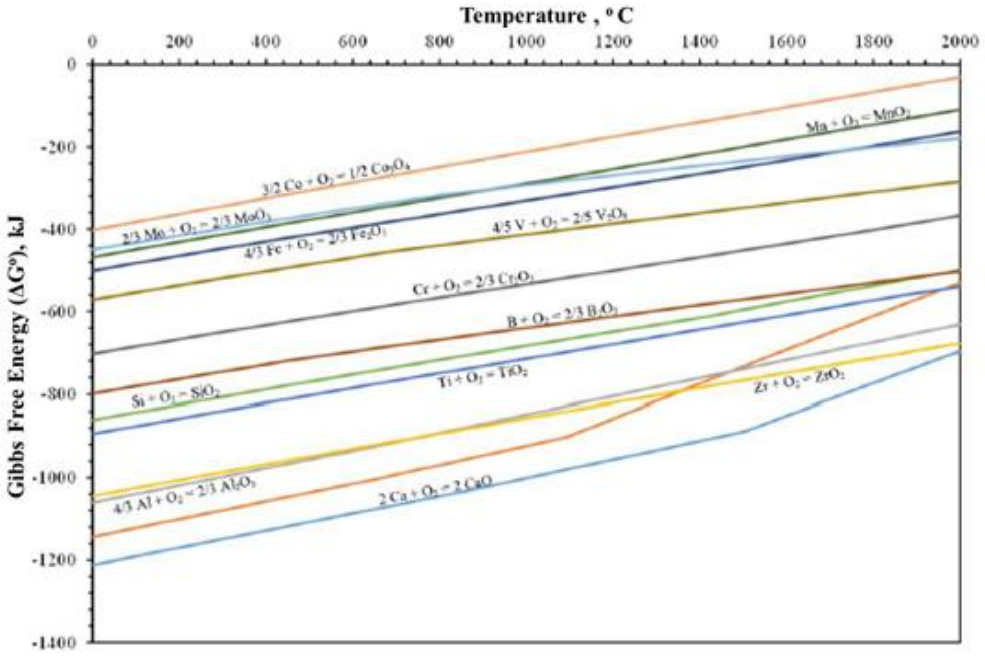

Figure 6.1 The Ellingham diagram (Alkan, 2014)

The Gibbs free energy changes of the reduction of various metal oxides by Al, Si, and Mg are given in Figure 6.2, Figure 6.3, and Figure 6.4, respectively. It can be seen in Figure 6.2 that metal oxides other than ZrO_2 can be reduced with Al. The reduction of ZrO_2 will not occur above about 500°C. CuO has the highest reduction tendency with Al over selected metals. The reduction tendency of metal oxides with Al from

low to high is given in the following order: ZrO_2, TiO_2, B_2O_3, Ta_2O_5, Nb_2O_5, Cr_2O_3, V_2O_5, WO_3, Fe_2O_3, MnO_2, MoO_3, NiO, Co_3O_4, CrO_3, and CuO.

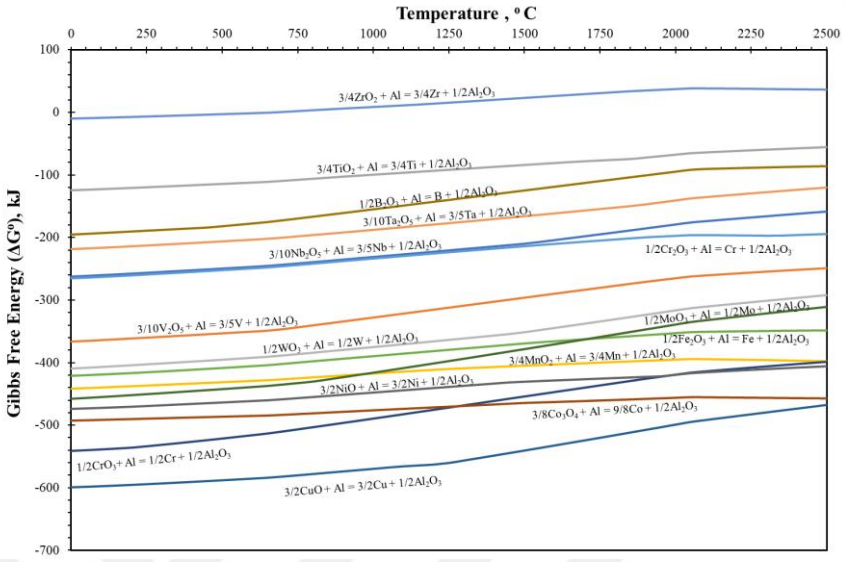

Figure 6.2 Standard free energy changes of reactions of various metal oxides with one mole of Al (HSC 6.2, 2007)

In Figure 6.3, it is seen that ZrO_2 and TiO_2 cannot be reduced at any temperatures, and B_2O_3 can only be reduced under 1900°C by Si. Considering the reduction tendencies of metal oxides with Si, similar behavior is observed with the reduction tendency with Al. Only the Gibbs Standard Energy changes of the reduction of TiO_2 and ZrO_2 have positive values.

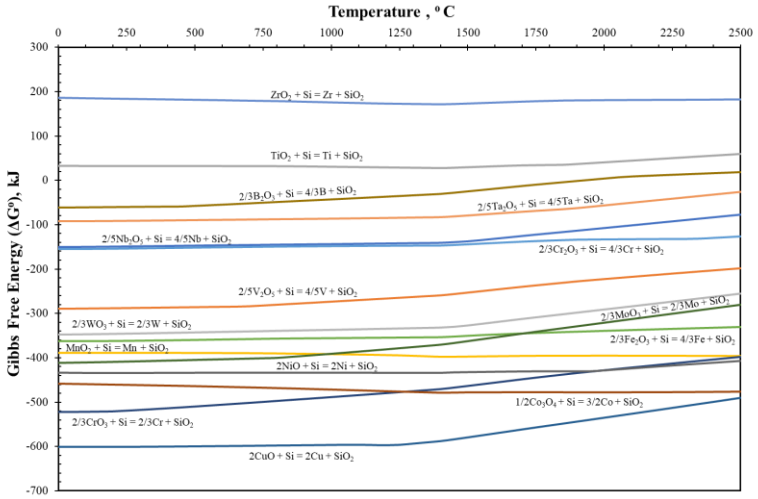

Figure 6.3 Standard free energy changes of reactions of various metal oxides with one mole of Si (HSC 6.2, 2007)

All selected metal oxides can be reduced with Mg. However, ZrO_2 cannot be reduced above 2250°C when considered in Figure 6.4. The reduction tendency of metal oxides with Mg from low to high is given in the following order: ZrO_2, TiO_2, B_2O_3, Ta_2O_5, Nb_2O_5, Cr_2O_3, V_2O_5, WO_3, Fe_2O_3, MnO_2, MoO_3, NiO, Co_3O_4, CrO_3, and CuO.

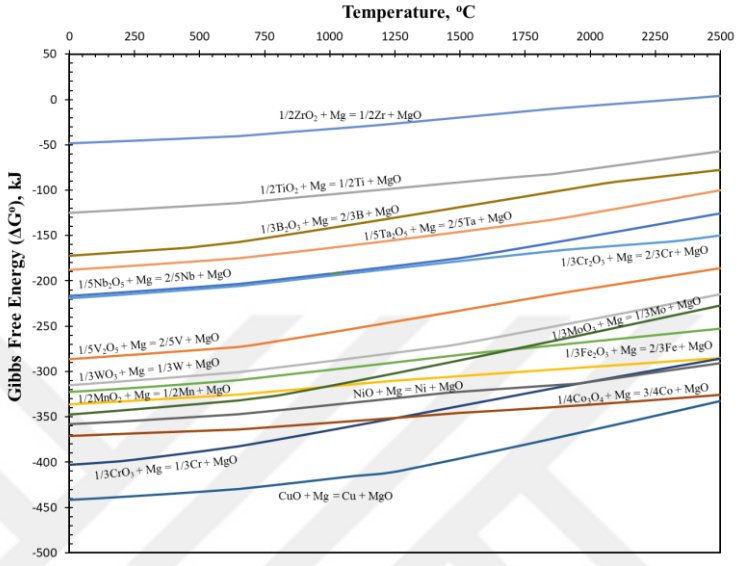

Figure 6.4 Standard free energy changes of reactions of various metal oxides with one mole of Mg (HSC 6.2, 2007)

There are two essential parameters in SHS reactions: the adiabatic temperature and the specific heat. The adiabatic temperature values ought to be greater than 1800K (1527°C) towards a self-propagating reactions. Therefore, all of the reactions may be realized as self-sustaining as a result of the thermochemical calculated values. Released energy is an important parameter for easily separating the metal and slag in the products to be produced as the outcome of the reaction. In order to have a controlled SHS reaction, the released energy must be between 2250-4500 J/g (Alkan, 2014). These two conditions must be provided in order to produce L-HEAs by SHS with estimated compositions.

The enthalpy, specific heat, and adiabatic temperature values of the selected L-HEA systems were calculated, and the results are given in Table 6.2. Theoretically desired parameters are provided when the obtained results are examined. The specific heat value of all alloy systems is in the range of 2250 to 4500 J/g. Likewise, the adiabatic temperature value is above 1527°C in all L-HEAs.

Table 6.2 Enthalpy, specific heat and adiabatic temperature values of the reactions with reductant type and ratio in L-HEA systems (HSC 6.2, 2007)

Alloy Systems	**Reductant Type and Ratio**	**$\Delta H°_{rxn,298K}$ (kJ)**	**Specific Heat (J/g)**	**T_{ad} (C)**
AlSiTiNbV	%80 Al %20 Si	-1095.54	2286.34	2053.80
AlSiTiNbV	%85 Al %15 Si	-1131.64	2354.89	2053.90
AlSiTiNbV	%100 Al	-1239.93	2558.18	2053.80
AlSiMgTiV	%100 Al	-793.29	2395.76	2003.90
AlSiMgTiMn	%100 Al	-767.41	2412.29	2019.70
AlSiMgTiCr (CrO_3)	%100 Al	-1266.91	3628.34	2478.70
AlSiMgTiCr (CrO_3)	%100 Si	-751.24	2280.31	1900.90
AlSiMgTiCr (CrO_3)	%100 Mg	-1482.09	3892.46	2826.90
AlSiMgTiMnCr (CrO_3)	%100 Al	-1861.94	3944.09	2736.50
AlSiMgTiMnCr (Cr_2O_3)	%100 Al	-1037.9	2464.72	2053.90
AlSiMgTiMnCrFe (CrO_3)	%100 Al	-2288.29	3952.76	2797.30
AlSiMgTiMnCrFe (Cr_2O_3)	%100 Al	-1464.25	2773.58	2053.80

6.2 SHS Experiment Results and Discussion

The equiatomic $AlSiTiME_IME_{II}$ (ME_I, ME_{II} = Mg, Nb, V, Mn, Cr, Fe) based, light metal containing high entropy alloys were generated by a SHS beginning with mixtures of metal oxide powder. A total of 15 experiments were carried out in accordance with the determined parameters. The parameters and results of the experiments for producing light metal containing HEAs by the SHS technique are given within Table 6.3.

Considering the results of SHS experiments given in Table 6.3, it is seen that metal-slag separation does not occur during the production of some alloys, even if the theoretically calculated specific heat value (Table 6.2) is sufficient. The theoretical specific heat values of SHS reactions are calculated as 2280, 2286, and 3892 J/g,

respectively in AlSiTiMgCr (Si-thermic), AlSiTiMgCr (Mg-thermic), and AlSiTiNbV (%80 Al + %20 Si thermic) alloys. During the calculation of the theoretical specific heat value, it is assumed that the HEAs are the ideal solution, and the enthalpy change of the solution is considered to be zero. If the molar enthalpy changes in the solution are positive, the enthalpy value and specific heat value of the SHS reactions will decrease, and the required limit value for metal-slag separation will not be reached. It is thought that SHS reactions did not occur due to the positive value of the molar enthalpy alteration of the solution. Within this reaction with one specific heat of 3892 J/g, Mg was used as the reductant. Due to the high melting temperature of MgO, the products could not be completely melted. The Mg-thermic SHS experiment was unsuccessful, as the products remained in solid form and did not form a liquid alloy. The adiabatic temperatures and the specific heat values of Mg-thermic SHS reactions were calculated between 2020-2054°C and 2355-2465 J/g. Both values are theoretically sufficient, but SHS reactions did not occur due to metal oxides' meager reduction potential that will form L-HEA as raw materials.

Table 6.3 Experimental results and parameters of L-HEA systems produced by SHS method

Target L-HEA	**Inspected Parameters**	**Parameter**	**Experimental Result**
AlSiTiNbV	Reductant ratio	%100 Al	Successful
AlSiTiNbV	Reductant ratio	%85 Al + %15 Si	No reaction
AlSiTiNbV	Reductant ratio / Crucible type	%80 Al + %20 Si / C + exoth. Sleeve	Metal-slag separation is insufficient
AlSiTiNbV	Crucible type	Small volume Cu	Metal-slag separation is insufficient
AlSiTiNbV	Crucible type	High volume Cu	Metal-slag separation is insufficient
AlSiTiMgCr	5th element difference / Reductant type	ME = Cr / Al- thermic	Successful
AlSiTiMgCr	Reductant type	Si- thermic / Mg- thermic	Metal-slag separation is insufficient
AlSiTiMgV	5th element difference	ME = V	Successful
AlSiTiMgMn	5th element difference	ME = Mn	No reaction
AlSiTiMgMnCr	6th element effect Cr raw material effect	utilization of Cr_2O_3	No reaction
AlSiTiMgMnCr	7th element effect Cr raw material effect	utilization of CrO_3	Successful
AlSiTiMgMnCrFe	7th element effect Cr raw material effect	utilization of Cr_2O_3	Successful
AlSiTiMgMnCrFe	7th element effect Cr raw material effect	utilization of CrO_3	Successful

The amount of material lost due to scattering and evaporation was between 0.36-37.8% by weight. In comparison, the alloy weights were between 13.1-59.3 g in the successful experiments. The amounts of alloys, slags, and lost material obtained as a result of the SHS experiments are illustrated in Table 6.4. It is visible that the alloy weights are less than the weights of slags. The weights of the lost materials are also relatively less than the slags'.

Table 6.4 The weights of alloys, slag, and lost material obtained from SHS experiments in estimated L-HEA systems.

Alloy Systems	**Reductant Type and Ratio**	**Metal (g)**	**Slag (g)**	**Loss (g)**
AlSiTiNbV	%100 Al	33.62	115.83	0.55
AlSiMgTiV	%100 Al	27.37	121.01	1.62
AlSiMgTiCr (CrO_3)	%100 Al	13.08	80.12	56.80
AlSiMgTiMnCr (CrO_3)	%100 Al	26.55	115.79	7.66
AlSiMgTiMnCrFe (CrO_3)	%100 Al	30.78	96.94	22.28
AlSiMgTiMnCrFe (Cr_2O_3)	%100 Al	59.28	88.81	1.91

In L-HEA systems, the configurational entropy values of the alloys were calculated according to the chemical compositions of the SHS alloys. The alloys are called high entropy alloys if the configurational entropy value is more than 1.5 R; in other words, more than 12.471 J/mol.K. Table 6.5 shows the configurational entropy values of the obtained alloys after SHS experiments, calculated according to their chemical compositions. By considering the calculated configurational entropy values, it is seen that the three produced alloys have high entropy. The other two alloy systems (AlSiMgTiV and AlSiMgTiCr (CrO_3)) belong to the medium entropy alloy group. These calculations estimate that the probability of solid solution phases in the microstructure of the produced SHS alloys is higher than that of intermediate compounds and mixtures of different phases.

Table 6.5 Entropies of obtained LHEA systems as a result of SHS reactions

Alloy Systems	**Reductant Type and Ratio**	**ΔS_{conf} (R)**
AlSiTiNbV	%100 Al	1.58
AlSiMgTiV	%100 Al	1.07
AlSiMgTiCr (CrO_3)	%100 Al	1.18
AlSiMgTiMnCr (CrO_3)	%100 Al	1.52
AlSiMgTiMnCrFe (CrO_3)	%100 Al	1.70
AlSiMgTiMnCrFe (Cr_2O_3)	%100 Al	1.67

6.2.1 AlSiTiME$_I$ME$_{II}$ (ME$_I$ME$_{II}$: MgCr / NbV / MgV) Alloy Systems

Samples were taken for analysis from the obtained alloy systems as a result of the SHS experiments. The chemical compositions of L-HEAs and their slags were examined by XRF analysis. By using chemical compositions and weights of products, distributions of the elements on the product are calculated in the following equation (6.1):

$$[\mathbf{DMe}]\ \mathbf{or}\ (\mathbf{DMe}) = \frac{([\%\mathbf{Me}]\ \mathbf{x\ weight\ of\ alloy\ or}\ (\%\mathbf{Me})\ \mathbf{x\ weight\ of\ alloy})}{(\mathbf{wt\%\ Me\ in\ initial\ mix\ x\ weight\ of\ initial\ mix})} \qquad (6.1)$$

where [D_{Me}] is the distribution rate of element in the alloy, (D_{Me}) is the distribution ratio of element in slag, [% Me] is the content of element in the alloy, and (% Me) is the content of element in slag. The dispersion of the elements was calculated on the products obtained by the SHS method.

The target alloys in the quintet AlSiTiME$_I$ME$_{II}$ system are AlSiTiNbV, AlSiTiMgCr, and AlSiTiMgV. The recovery efficiencies of elements except for the reductant were obtained at lower values when the distribution ratios of the elements in three L-HEA alloy systems were examined, shown in Figure 6.5. The highest metal recovery efficiencies were calculated as 46.5% Nb, 39.8% V, 31.6% Ti, and 25.1% Cr, respectively. The recovery efficiency of Cr is lower than other metals because the specific heat value of the reaction of CrO_3 with Al is higher than 4500 J/g, and it causes the scattering rate to be high due to an uncontrolled reaction. Cr_2O_3 can also be chosen

as another Cr source in the raw material instead of CrO_3. Nevertheless, the calculated specific heat and adiabatic temperature values of Cr_2O_3 are insufficient for the combustion wave identified as a solid flame to proceed spontaneously.

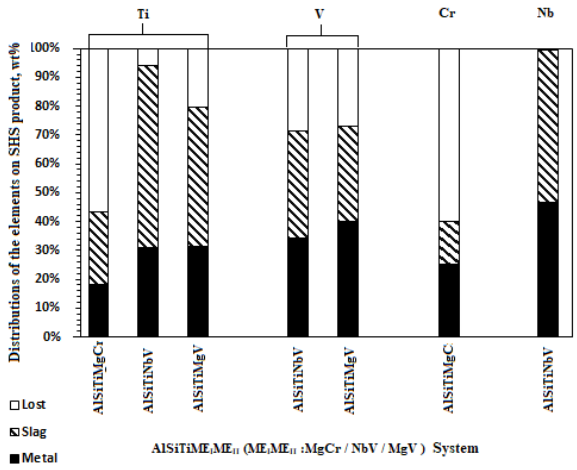

Figure 6.5 The distributions of elements on the SHS products in $AlSiTiME_IME_{II}$

The SHS experiment, in which the total loss rate due to scattering or evaporation is the lowest, was obtained by producing AlSiTiNbV alloy. The weight of the SHS alloy was lower than expected because the reduction potentials of TiO_2, Nb_2O_5, and V_2O_5 used as raw materials are low. The chemical compositions of the SHS alloys calculated by SEM/EDS method are exemplified in Table 6.6.

Table 6.6 Chemical composition of $AlSiTiME_IME_{II}$ estimated L-HEAs calculated by SEM/EDS (atomic %)

Estimated L-HEAs	Al	Si	Ti	ME_I	ME_{II}	O
AlSiTiNbV	26.59	20.03	6.61	28.50	17.14	0.00
AlSiTiMgCr	34.99	24.65	16.59	0.29	20.45	2.30
AlSiTiMgV	44.23	23.59	12.02	0.40	18.83	0.00

In Table 6.6, it can be seen that Mg contents were much lower than the expected values. In the SHS experiments, only metallic Al powders were added as reducing agents, and metallic Si and Mg added to the raw material were used to obtain the estimated L-HEAs compositions. It is thought that the reasons for the Mg content in the SHS alloys to be much lower than the estimated composition are the acting of Mg powders as the reducing agents and the evaporation of Mg due to the high adiabatic

temperatures. It was observed that Ti content was also lower than expected in the three target L-HEA compositions. When the compositions of the alloys are examined, it is seen that alloys with equiatomic compositions cannot be produced by the SHS method. In addition, when the microstructure images given in Figure 6.6 are examined, it is seen that a homogeneous microstructure also cannot be obtained by the SHS method.

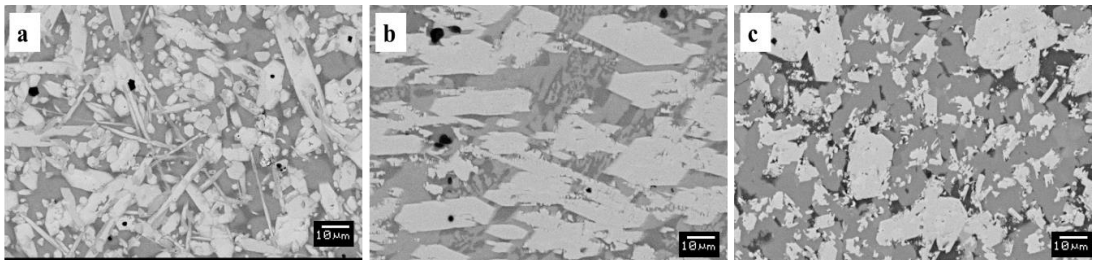

Figure 6.6 Back-scattered electron microstructure (BSE) images of a) AlSiTiNbV, b) AlSiTiMgCr, and c) AlSiTiMgV L-HEAs produced by the SHS method

The compositions of the phases observed in the AlSiTiNbV microstructure, produced by the SHS method, were examined by SEM/EDS technique. The back-scattered electron image with the selected areas is given in Figure 6.7, and the chemical compositions of these selected areas are given in Table 6.7.

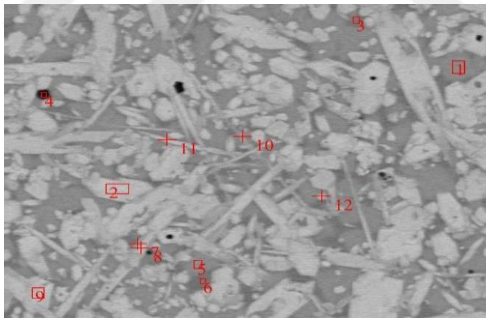

Figure 6.7 The back-scattered electron (BSE) images of estimated AlSiTiNbV (1000 X)

Table 6.7 Chemical composition of AlSiTiNbV estimated L-HEA calculated by SEM/EDS (at.%)

Element	Regions (1000 X)											
at.%	1	2	3	4	5	6	7	8	9	10	11	12
Al	64.78	2.62	35.89	63.03	65.46	38.08	3.17	3.78	2.08	58.42	11.90	9.10
Si	0.05	30.52	4.74	1.25	0.00	2.41	31.39	31.56	31.59	4.33	27.25	27.11
Ti	2.71	7.52	4.61	1.49	2.48	5.03	8.46	7.82	7.74	3.26	7.57	8.29
Nb	26.58	43.19	6.18	8.00	26.57	4.40	35.17	37.55	41.98	28.32	34.83	27.87
V	4.46	15.06	35.55	4.46	3.62	36.65	21.30	19.03	16.45	5.43	18.17	25.12
Fe	0.47	0.18	9.69	0.87	0.39	10.13	0.51	0.26	0.17	0.24	0.29	1.83

When the data in Table 6.7 are examined, it is seen that Ti is relatively lower than others. The compositions of regions 1, 5, and 10 are rich in Nb and Al, while regions 3 and 6 are rich in Al and V. It is thought that region 4 is composed of Al_2O_3 oxide. It is seen that other regions are relatively rich in Nb, Si, and V. It has been found that most of the phases were on a two-element basis, some of the phases were on a three-element basis, and some phases in small amounts are rich in four-element basis. However, it was observed that there were not any phases having these five elements in the equiatomic ratio. The possible phases and their average compositions were investigated using the Thermo-Calc program. Considering the average compositions, where the composition consists of two elements by weight, it is thought that the regions rich in Al and Nb belong to the AL3TI phase, while the regions rich in Al and V belong to the ordered B2 phase. It is thought that the Nb, Si, and V-rich regions are composed of TA5SI3 + CR3S or TA5SI3 + B2 + ALTI phase mixtures according to their compositions. It is thought that the region consisting of Nb, Si, V, and Al consists of the TA5SI3 + B2 phase mixture, while four elements constitute the composition by weight.

The XRD analysis result of the obtained AlSiTiNbV alloy is given in Figure 6.8. According to phase analysis, the AlSiTiNbV comprises five different phases. It is concluded that the matching phases were Nb_5Si_3, Ti_5Si_3, AlTi, SiV_3, and Al_3Nb. According to Thermo-Calc calculation, the structural design of these phases was $D8_l$, A15, $D0_{22}$, $L1_0$, and $D8_8$, respectively. The phases detected by XRD analysis and possible phases obtained by Thermo-Calc analysis overlapped.

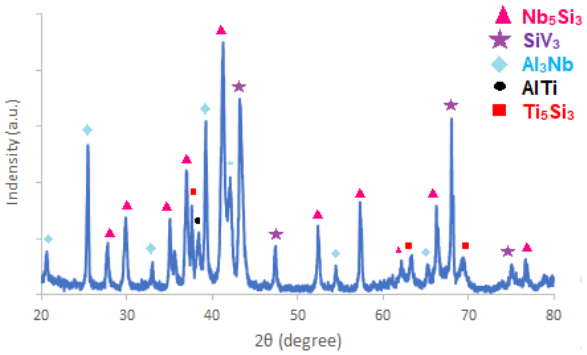

Figure 6.8 XRD patterns of the estimated AlSiTiNbV alloy

The back-scattered electron image of the AlSiMgTiCr alloy with the selected areas is given in Figure 6.9, and the chemical compositions of these selected areas are given in Table 6.8.

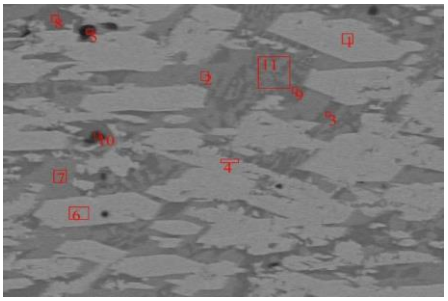

Figure 6.9 The back-scattered electron (BSE) images of estimated AlSiMgTiCr (1000 X)

Table 6.8 Chemical composition of AlSiMgTiCr estimated L-HEA calculated by SEM/EDS (at.%)

Element	Regions (1000 X)										
at.%	1	2	3	4	5	6	7	8	9	10	11
Fe	0.21	0.93	0.46	0.21	0.25	0.32	1.49	0.18	0.31	0.32	0.91
Mg	0.03	0.31	0.55	0.05	10.38	0.08	0.35	0.60	0.53	12.10	0.49
O	2.06	1.93	0.72	0.97	24.54	2.38	1.59	0.71	1.24	23.52	1.65
Al	4.06	65.65	70.84	6.24	56.19	4.07	65.75	71.65	71.49	57.40	68.48
Si	43.39	4.10	2.40	36.62	1.88	43.39	5.11	2.07	1.94	0.82	2.86
Ti	21.22	4.31	9.57	34.55	3.16	21.16	2.46	13.55	13.64	2.86	7.37
Cr	29.02	22.76	15.47	21.37	3.61	28.61	23.25	11.26	10.85	2.99	18.24

It is seen in Table 6.8 that there were not any phases having the five elements in an equiatomic ratio, as with AlSiTiNbV alloy. The bright areas in Figure 6.9 consist of heavier alloying elements like Cr and Ti, while dark areas are composed of lighter alloying elements like Al, Mg, and Si. Accordingly, the composition of bright areas labeled as 1, 4, and 6 are rich in Si, Ti, and Cr, whereas the composition of dark areas labeled as 3, 8, 9, and 11 is rich in Al, Si, and Ti. It is seen that the labeled regions 2 and 7 include approximately 65.70% Al and 23.00% Cr. The labeled region five consists of Al_2O_3, and the labeled region 10 consists of Al_2O_3 and MgO mixtures. The possible phases and their average compositions were also investigated using the Thermo-Calc program. Considering the intermediate compositions, there could be several intermetallic phases in the microstructures like AL3TI, CR3SI1, CR5SI3, and ZR5SI5.

The XRD analysis result of the AlSiMgTiCr alloy is given in Figure 6.10. According to phase analysis, the AlSiMgTiCr is composed of six phases. The matched phases followed as Ti_9Al_{23}, Cr_3Si (A15), $Cr_5Si_3(D8_m)$, Al_8Fe_2Si, $Ti_5Si_3(D8_m)$, and Al_6Ti_{19}.

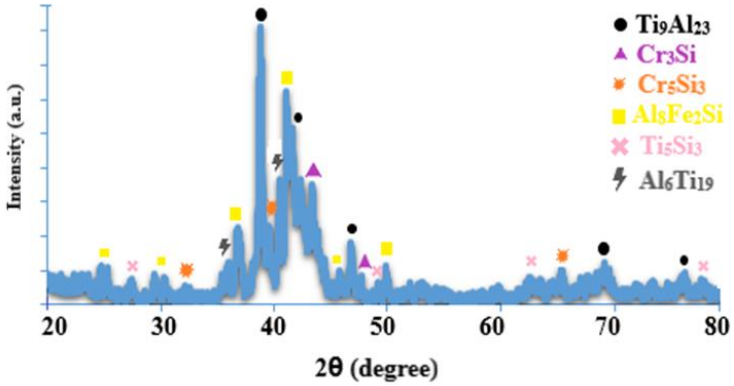

Figure 6.10 XRD patterns of the estimated AlSiMgTiCr alloy

The back-scattered electron image of the AlSiMgTiV alloy with the selected areas is given in Figure 6.11, and the chemical compositions of these selected areas are given in Table 6.9.

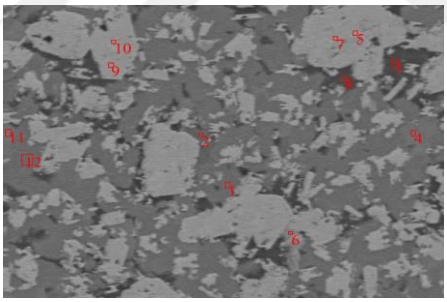

Figure 6.11 The back-scattered electron (BSE) images of estimated AlSiMgTiV (1000 X)

Table 6.9 Chemical composition of AlSiMgTiV estimated L-HEA calculated by SEM/EDS (at.%)

Element	Regions (1000 X)											
at.%	1	2	3	4	5	6	7	8	9	10	11	12
Fe	0.21	0.61	0.12	5.16	0.21	1.66	0.14	0.10	0.11	0.18	1.67	0.22
Al	63.99	70.34	85.92	69.40	2.07	29.95	7.86	66.50	1.97	2.22	69.84	66.70
Si	8.68	11.03	3.83	9.17	46.64	40.49	42.86	16.22	46.23	45.98	6.08	6.00
Ti	12.03	2.89	3.54	6.43	18.82	8.74	17.07	5.04	17.93	19.09	9.55	12.43
V	14.70	14.56	4.75	9.03	32.03	18.46	28.92	10.10	33.43	32.38	12.46	14.41
Mg	0.39	0.56	0.71	0.42	0.02	0.29	0.91	0.43	0.07	0.04	0.40	0.24

The SEM/EDS analyses showed that AlSiMgTiV consisted of a multiphase microstructure and four phases with different contrast in the alloy (Figure 6.11). Therefore, it is concluded that AlSiMgTiV alloy could not be produced in equiatomic composition, and a homogeneous structure is not formed. It is seen in Table 6.9 that there was a trace of Mg in the microstructure. The analyses showed that the average composition of the bright areas represented as 5, 7, 9, and 10 contain 31.69% V, 45.43% Si, and 18.22 % Ti, respectively. The compositions of darker areas labeled as 1, 11, and 12 are rich in Al, V, and Ti. In addition to these areas, the area labeled as 3 is included 85.92% Al, 4.75% V, and 3.83% Si. The areas labeled 2 and 4 have similar chemical compositions. The possible phases and their average compositions were also investigated using the Thermo-Calc program. Considering the intermediate compositions, there could be several intermetallic phases in the microstructures like W5SI3, AL3TI, and M5SI3.

The XRD analysis result of the AlSiMgTiV alloy is given in Figure 6.12. According to phase analysis, the AlSiMgTiV is composed of four phases. The matched phases were Si_3V_5, AlTi, Al_3V, and $MgAl_2O_4$. According to Thermo-Calc calculation, the structural design of these phases was $D8_m$, $L1_0$, $D0_{22}$, and $H1_1$.

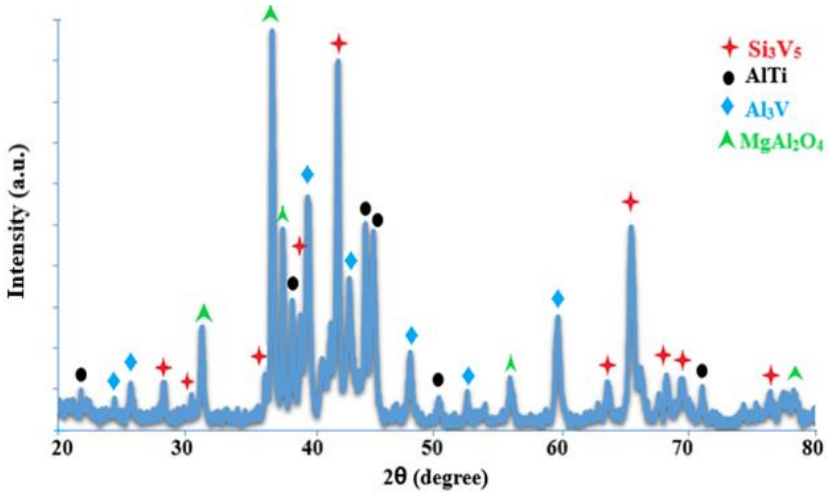

Figure 6.12 XRD patterns of the estimated AlSiMgTiV alloy

Comparative Vickers hardness results of obtained $AlSiTiME_IME_{II}$ (ME_IME_{II}: MgCr /NbV/MgV) alloys are exemplified in Figure 6.13. The lowest hardness values are obtained in AlSiMgTiV alloy, while the highest hardness values were obtained in AlSiTiNbV alloy. It was observed that Mg was present in a minor amount in the alloy

systems, and the Nb element improved the hardness of the alloy when the effect of MgV/NbV element pairs on hardness values was examined. It is seen that the Cr element enhanced the hardness of the alloy when the impact of MgV/MgCr element pairs on hardness is reviewed. Standard deviation values were measured as 3.4% in AlSiMgTiCr, 3.5% in AlSiTiNbV, and 5.4% in AlSiMgTiV.

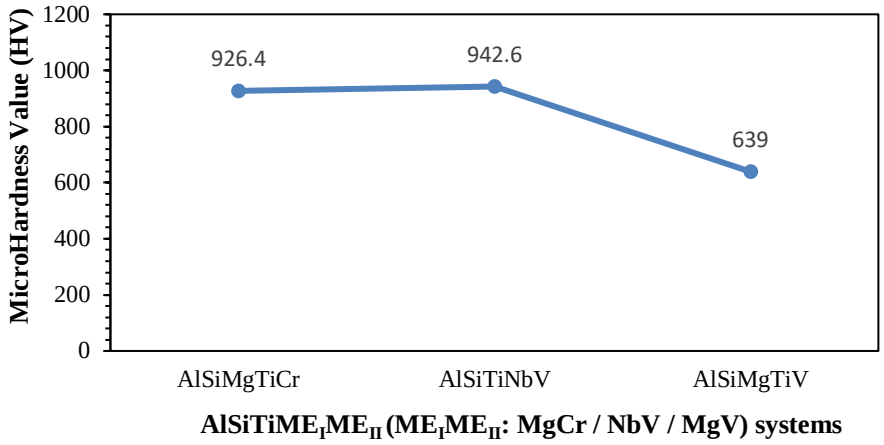

Figure 6.13 Vickers microhardness analysis results of AlSiTiME$_I$ME$_{II}$ (ME$_I$ME$_{II}$: MgCr/NbV/MgV) systems

6.2.2 Effect of the Number of Principal Elements on AlSiTiMg-based Alloy Systems

The other parameter investigated is the number of the principal elements and their effects on the properties of the alloy. These examinations were carried out by adding different combinations of Cr, Mn, and Fe elements into the AlSiTiMg alloy system. The SHS reaction did not take place for the production of AlSiTiMgMn, and a complete SHS reaction was achieved for AlSiTiMgCr when the addition of CrO_3 was provided as a Cr source in the starting mixture. The successful SHS reactions were also realized for producing AlSiTiMgCrMn and AlSiTiMgCrMnFe alloys. The distributions of Ti, Cr, Mn, and Fe on the products are given in Figure 6.14.

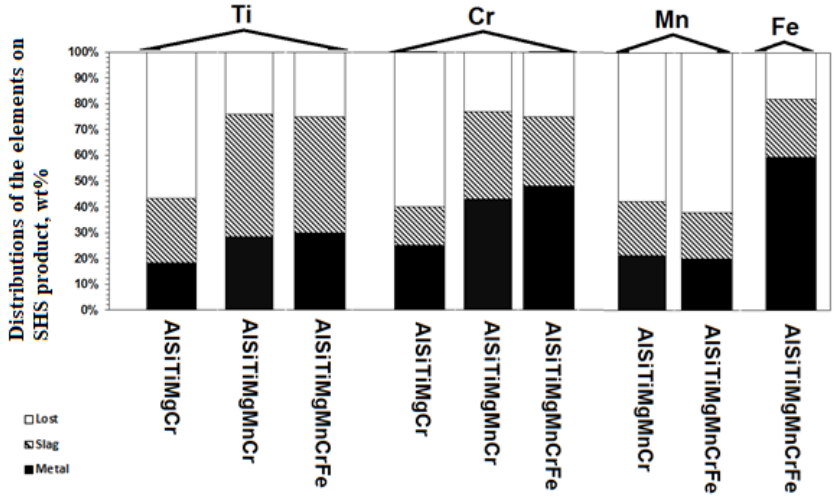

Figure 6.14 Distributions of metals on SHS products obtained where the effects of the number of principal elements were investigated

As seen in Figure 6.14, the recovery efficiencies of metals increase as the count of principal elements within AlSiTiMg alloy rises. The highest metal recovery efficiencies were obtained as 59.7% Fe, 45.1% Cr, 30.0% Ti, and 21.3% Mn, respectively. The amounts of the lost materials due to scattering and evaporation were high in all three alloys. Most of the amount of Ti is found in the slag, while most of Mn's is lost by evaporation. The chemical compositions of the obtained L-HEAs are given in Table 6.10. Mg could not be obtained in the final composition in all three alloys. It has been observed that the amounts of Al and Si used as reductants are higher than the target alloy compositions due to the inadequacy of reducing other elements.

Table 6.10 Chemical composition of SHS products obtained where the effects of the number of principal elements were investigated (atomic %)

Estimated L-HEA	Al	Si	Ti	Mg	Cr	Mn	Fe	O
AlSiMgTiCr	34.99	24.65	16.59	0.29	20.45	-	-	2.30
AlSiMgTiMnCr	33.56	29.37	10.07	0.18	16.28	9.21	-	1.34
AlSiMgTiMnCrFe	23.10	26.93	8.83	0.10	15.40	6.50	17.24	1.43

SEM/EDS and XRD analysis results of AlSiTiMgCr alloy are exemplified in Figure 6.9, Figure 6.10, and Table 6.8, respectively, and the discussions of these results are given in the previous section in detail. Therefore, the results of the other two alloys will be examined in this section. The BSE view of the AlSiTiMgCrMn alloy, produced

by using CrO_3 as the Cr-source, with the selected areas is given in Figure 6.15, and the chemical compositions of these selected areas are given in Table 6.11.

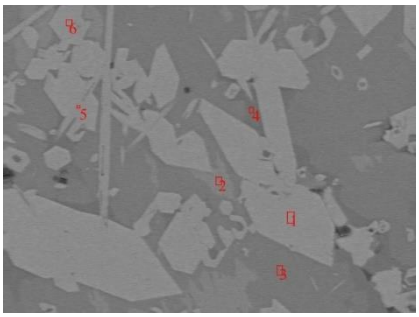

Figure 6.15 The back-scattered electron view of estimated AlSiTiMgCrMn alloy produced with CrO_3 addition (1000 X)

Table 6.11 Chemical composition of estimated AlSiTiMgCrMn alloy produced with CrO_3 addition calculated by SEM/EDS (at.%)

Element	Regions (1000 X)					
at.%	1	2	3	4	5	6
Mg	0.07	0.25	0.27	0.27	0.10	0.11
Cr	27.18	16.91	10.01	7.63	19.93	26.60
O	1.97	1.47	0.71	0.77	1.40	1.67
Al	2.00	46.68	60.57	59.89	5.10	1.88
Si	45.32	19.75	13.71	19.32	38.73	45.67
Ti	18.91	1.01	0.50	2.00	30.59	19.04
Mn	4.56	13.93	14.24	10.12	4.15	5.03

The SEM/EDS analysis in Figure 6.15 showed that the AlSiTiMgCrMn alloy produced with CrO_3 addition consisted of a multiphase microstructure, and there were four phases with different contrast in the alloy. Therefore, it can be said that this alloy could not be produced in equiatomic composition, and a homogeneous structure is not formed. It is seen in Table 6.11 that there was a trace of Mg in the microstructure. The analyses demonstrated that the average composition of the bright areas labeled 1 and 6 contains 26.89% Cr, 45.49% Si, and 18.97% Ti. In addition, the labeled region as 5 involves 30.59% Ti, 38.73% Si, and 19.93% Cr. The regions represented as 2, 3, and 4 were rich in Al, Mn, Si, and Cr elements with varying compositions. Depending on the Thermo-Calc analysis, the microstructure could have several intermetallic phases, such as AL8MN5, CR3SI1, and M5SI3.

The XRD analysis result of the AlSiTiMgCrMn alloy produced with CrO_3 addition is given in Figure 6.16. According to the analysis, the AlSiTiMgCrMn alloy is

composed of four phases. It was found that the matching phases were $Ti_7Al_5Si_{12}$, $Al_{10}Mn_3$, Cr_3Si (A15), and $TiMnSi_2$.

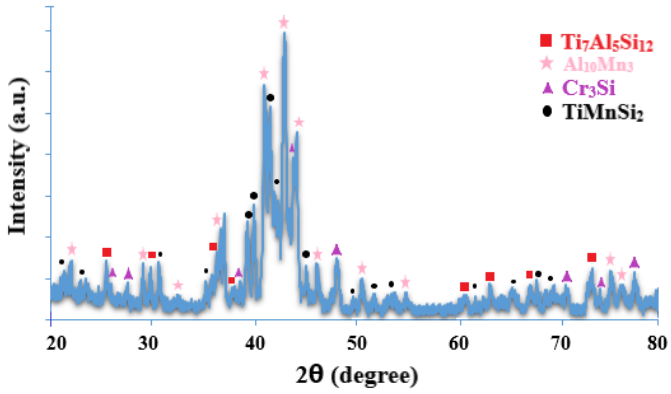

Figure 6.16 XRD patterns of the estimated AlSiTiMgCrMn alloy produced with CrO_3 addition

To examine the influences of the seventh principal element on the features of alloys, a Fe source was added to the raw mixtures to obtain AlSiTiMgCrMnFe alloy. Two types of Cr sources were used separately in the raw materials: CrO_3 and Cr_2O_3. Both raw material mixtures provide the thermodynamic requirements for realizing a SHS reaction. The distribution of the elements onto the products is given in Figure 6.17.

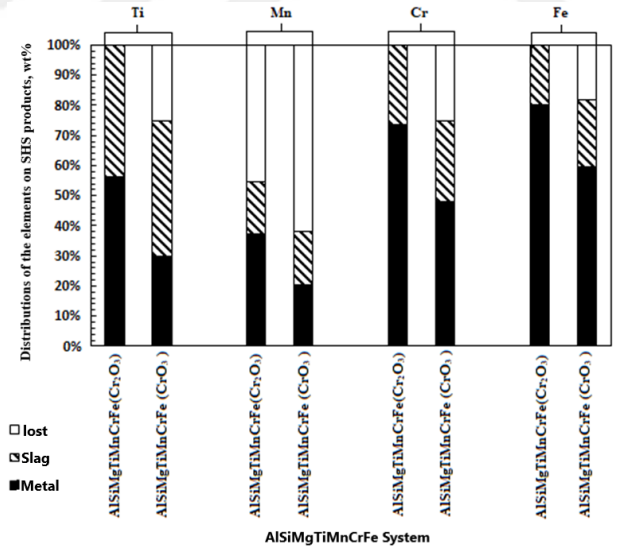

Figure 6.17 The distributions of the elements on AlSiTiMgCrMnFe alloys obtained by using different Cr sources

As exemplified in Figure 6.17, superior metal recovery amounts were obtained when Cr_2O_3 was used as the Cr source in the raw material. The order of metal recovery efficiencies from high to low was obtained as Fe, Cr, Ti, and Mn, respectively, in

experiments using both raw material mixtures. The highest metal recovery efficiencies were calculated as 99.6% Fe, 76.6% Cr, 56.2% Ti, and 37.4% Mn. The Mn recovery efficiencies have been realized at lower levels, and a large amount of Mn added to the raw material mix passes into the loss part. The BSE images of the obtained AlSiTiMgCrMnFe alloys are given in Figure 6.18.

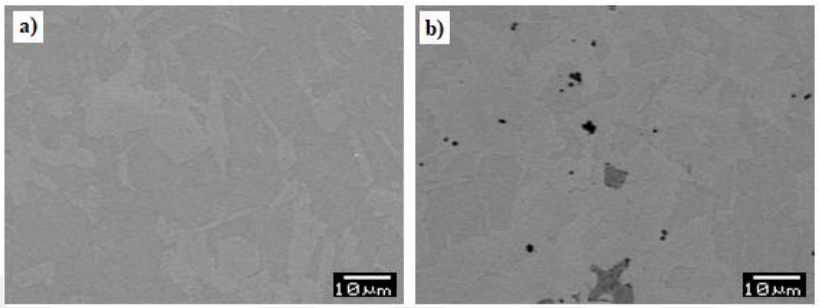

Figure 6.18 Back-scattered electron microstructure images of AlSiTiMgCrMnFe alloys produced using a) Cr_2O_3, b) CrO_3 as the Cr-source

By looking at Figure 6.18, it is seen that the two microstructures have similar appearances, and the most obvious difference is that the black regions are more intense in the microstructure of the alloy in which CrO_3 is used as raw material. The possible phases and their average compositions were also investigated using the Thermo-Calc program. Considering the intermediate compositions, the microstructures of alloys could have several phases like BCC solid solutions, M5SI3, AL8MN5, and CR3SI1. The BSE view of the AlSiTiMgCrMnFe alloy produced by using Cr_2O_3 as the Cr-source with the selected areas is given in Figure 6.19, and the chemical compositions of these selected areas are given in Table 6.12.

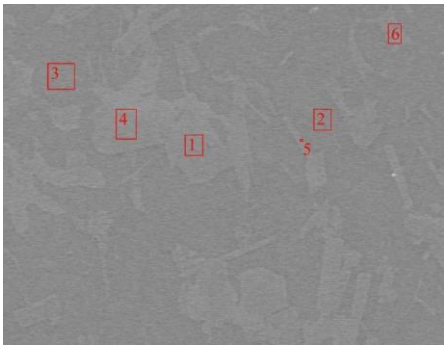

Figure 6.19 The BSE view of the AlSiTiMgCrMnFe alloy generated by used Cr_2O_3 as the Cr-source (1000 X)

Table 6.12 Chemical composition of the AlSiTiMgCrMnFe alloy produced by using Cr_2O_3 as the Cr-source calculated by SEM/EDS (at.%)

Element	Regions (1000 X)					
At.%	1	2	3	4	5	6
Fe	8.33	20.85	20.75	12.68	12.69	27.29
Al	4.50	41.91	41.20	10.49	15.52	35.42
Cr	23.66	10.59	12.26	20.30	19.55	6.69
Si	41.79	13.73	14.08	37.01	33.85	16.14
Mn	4.27	9.46	8.92	5.37	5.95	7.25
O	1.28	1.09	0.62	1.34	1.23	0.59
Mg	0.01	0.25	0.30	0.03	0.13	0.33
Ti	15.89	1.41	1.44	12.45	10.77	5.53

It can be sighted in Table 6.12 that the composition of regions labeled 2 and 3 were rich in Fe, Al, Cr, and Si elements, while the composition of the region labeled 6 was rich in Fe, Al, Si, and Mn elements. The chemical compositions of regions labeled 1, 4, and 5 were rich in Cr, Si, Fe, and Ti with different compositions.

The XRD analysis result of the AlSiTiMgCrMnFe alloy obtained using Cr_2O_3 as the Cr-source is given in Figure 6.20. According to phase analysis, this alloy comprises six phases: Al_8Mn_5, $AlMn_{0.75}Fe_{2.25}$, $Mn_4Ti_2Si_5$, $MgAl_2O_4(H1_1)$, Al_3SiCr, and $CrFe_8Si$.

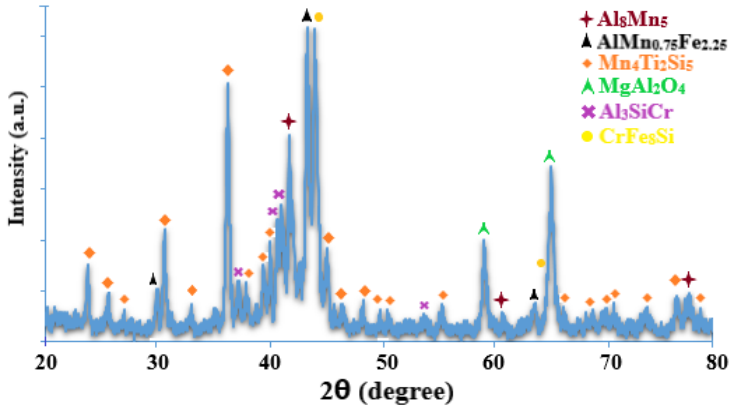

Figure 6. 20 XRD patterns of AlSiTiMgCrMnFe alloy obtained using Cr_2O_3 as the Cr-source

The BSE view of the AlSiTiMgCrMnFe alloy generated by used CrO_3 as the Cr-source with the selected areas is given in Figure 6.21, and the chemical compositions of these selected areas are given in Table 6.13.

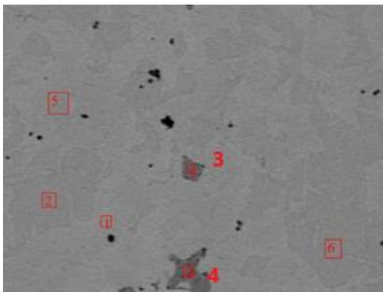

Figure 6.21 The BSE view of the AlSiTiMgCrMnFe alloy generated by used CrO_3 as the Cr-source (1000 X)

Table 6.13 Chemical composition of the AlSiTiMgCrMnFe alloy produced by using CrO_3 as the Cr-source calculated by SEM/EDS (at.%)

Element	Regions (1000 X)					
At.%	1	2	3	4	5	6
Fe	14.57	20.32	0.74	1.14	5.69	19.91
Al	12.77	40.74	0.26	0.85	2.42	40.93
Cr	19.51	11.58	2.31	3.05	22.74	11.95
Mg	0.06	0.08	0.04	0.08	0.06	0.24
Ti	11.06	1.49	93.40	87.31	26.30	1.38
Mn	5.13	9.39	0.43	0.65	2.89	8.87
Cu	0.33	0.72	0.35	0.28	0.26	0.65
O	1.17	1.19	1.14	3.56	1.01	1.12
Si	35.39	14.49	1.35	3.08	38.62	14.96

It can be seen in Table 13 that the labeled areas 2 and 6 are composed of Fe, Al, and Cr elements, respectively. While the labeled areas 3 and 4 consist of Ti by weight. Moreover, the EDS analysis indicated that 19.51% Cr, 35.39% Si, and 14.57% Fe are present in the labeled area as 1. In addition, 26.30% Ti, 22.74% Cr, and 38.62% Si are located in labeled area 5.

The XRD analysis result of the AlSiTiMgCrMnFe alloy obtained using CrO_3 as the Cr-source is given in Figure 6.22. According to phase analysis, this alloy comprises five phases: $CrFe_8Si$, Al_8Mn_5, $AlMn_{0.75}Fe_{2.25}$, $Cr_{0.78}Fe_{2.22}Si_2$, and $Mn_4Ti_2Si_5$.

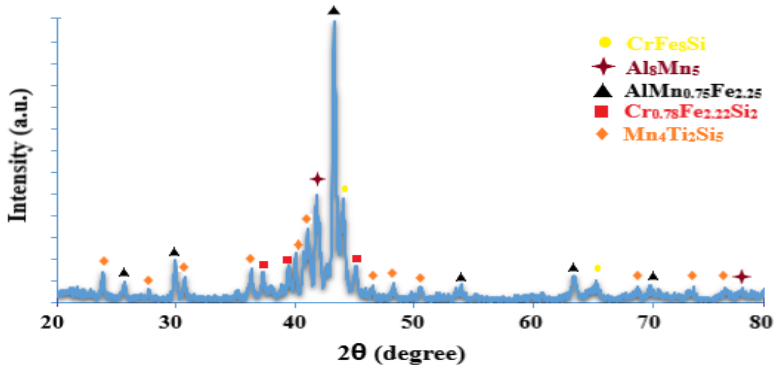

Figure 6.22 XRD patterns of AlSiTiMgCrMnFe alloy obtained using CrO_3 as the Cr-source

The obtained Vickers microhardness values of alloys where the effects of the number of principal elements were investigated were given in Figure 6.23. It is seen that other alloys except AlSiTiMgCrMn alloy have a hardness value of about 900 HV. The hardness was decreased with the addition of Mn into AlSiTiMgCr alloy. Although the Fe element improved the hardness of AlSiTiMgCrMn alloy, the AlSiTiMgCr alloy hardness value could not be reached. It was determined that a higher hardness value was obtained in the alloy using Cr_2O_3 when the effect of using different Cr oxide raw materials on hardness was examined.The standard deviation values of the hardnesses were measured as follows: 3.4% for AlSiTiMgCr, 2.3% for AlSiTiMgCrMn, 1.5% for AlSiTiMgCrMnFe (CrO_3 containing mixture), and 5.2% for AlSiTiMgCrMnFe (Cr_2O_3 containing mixture), respectively.

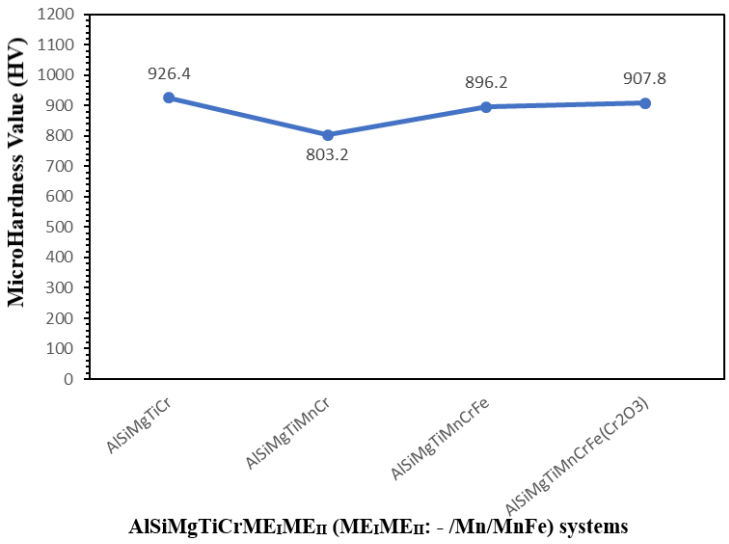

Figure 6.23 Vickers microhardness analysis results of SHS products obtained where the effects of the number of principal elements were investigated

CHAPTER 7

CONCLUSIONS

In this thesis, the estimated AlSiTiME$_I$ME$_{II}$-based (ME$_I$, ME$_{II}$ = Mg, Nb, V, Mn, Cr, Fe) light metal containing high entropy alloys were produced using a self-propagating high-temperature synthesis method, which is highly energy efficient, fast, and low-cost production technique. The experimental studies have been accomplished into three sections, Thermodynamic Analysis, SHS Reactions, and Characterization.

Thermodynamic analyses of the alloy systems were made using HSC Chemistry 6.2 and Thermo-Calc software and their related database. During the examinations, the "Reaction Equations" and "Heat and Material Balances" modules within the HSC Chemistry 6.2 software and the "One Axis Equilibrium" template of Thermo-Calc software were used. Using these modules, the free energy, enthalpy, adiabatic temperature, and specific heat (J / g) values of the reactions were calculated.

The examined parameters during the studies on the production of alloys whose compositions were determined as a result of thermodynamic studies by the SHS method are reductant types and their ratios, number of principal elements, and types of the Cr-source in the raw mixtures. The used raw materials in the SHS experiments were composed of metal oxide powders (TiO_2, V_2O_5, Nb_2O_5, MnO_2, Cr_2O_3, CrO_3, Fe_2O_3) and reductants (metallic Al, Si, and Mg powders). Raw material powder mixtures were weighed with a total weight of 150 g and mixed for 15 minutes, then fed into a crucible made of copper and compressed. SHS reactions were initiated by passing an electric current through the resistance wire placed on the surface of the raw material powder mixture in the Cu crucible. After the SHS reactions were completed, the crucible was rapidly cooled with water, the alloys and slags were separated, and their characterization was carried out.

The microstructure and mechanical properties of obtained L-HEAs were investigated through extensive characterization studies with scanning electron microscopy (SEM), X-ray diffraction (XRD), X-ray fluorescence (XRF), and microhardness (micro-Vickers) test device. Overall conclusions of this study, based

on the obtained results of experiments, are as follows:

1. A total of 15 experiments were carried out in accordance with the determined parameters. It was concluded that the theoretically calculated specific heat value could not be obtained experimentally when the experimental results were compared with the thermodynamic results' data. The specific heat values are calculated theoretically as 2280, 2286, and 3892 J/g in AlSiTiMgCr (Si-thermic), AlSiTiMgCr (Mg-thermic), and AlSiTiNbV (%80 Al + %20 Si thermic) alloys. However, it has been concluded that the specific heat values of the SHS experiments are insufficient due to incomplete metal-slag separation. Higher theoretical specific heat values could be obtained when Mg was used as the reductant. However, the products would not melt completely because the melting temperature of MgO is higher than the theoretical adiabatic temperature values. The SHS reactions did not occur even if the theoretical conditions were met, where the theoretical adiabatic temperatures were between 2020-2054°C, and the theoretical specific heat values were 2355-2465 J/g. Out of a total of 15 experiments, only six experiments have been successfully carried out. The estimated AlSiTiNbV alloy, produced by reduction with metallic Al, possessed the configurational entropy value of 1.58. The metal recovery efficiencies were obtained at 46.5% Nb, 34.1% V, and 31.1% Ti. The estimated AlSiTiNbV alloy is composed of five different phases. These phases are Nb_5Si_3, Ti_5Si_3, AlTi, SiV_3, and Al_3Nb. According to Thermo-Calc calculation, the structural design of these phases was $D8_l$, A15, $D0_{22}$, $L1_0$, and $D8_8$. The highest hardness value is obtained in the estimated AlSiTiNbV alloy as 942.6 HV. Nb element has improved the hardness of the alloy.

2. The estimated AlSiTiMgCr alloy produced using CrO_3 as the Cr-source and metallic Al as the reducing agent possessed the configurational entropy value of 1.18. This alloy system fell into the medium entropy alloy group. The metal recovery efficiencies were calculated as 25.1% Cr and 18.2% Ti in this alloy. According to phase analysis, the estimated AlSiTiMgCr alloy produced using CrO_3 as the Cr-source comprises six phases: Ti_9Al_{23}, Cr_3Si (A15), $Cr_5Si_3(D8_m)$, Al_8Fe_2Si, $Ti_5Si_3(D8_m)$ and Al_6Ti_{19}. The second highest hardness value is

obtained in the estimated AlSiTiMgCr alloy produced using CrO_3 as the Cr-source as 926.4 HV. It is seen that the Cr element enhanced the hardness of the alloy.

3. The estimated AlSiTiMgV alloy produced by reduction with metallic Al had the configurational entropy value of 1.07 due to the trace amount of Mg. This alloy also fell into the medium entropy alloy group. The metal recovery efficiencies were 39.8% V and 31.6% Ti. The different contrasts in the microstructure of this alloy showed that there were four phases: Si_3V_5, AlTi, Al_3V, and $MgAl_2O_4$. According to Thermo-Calc calculation, the structural design of these phases was $D8_m$, $L1_0$, $D0_{22}$, and $H1_1$. The lowest hardness value of 639 HV is obtained in this estimated AlSiTiMgV alloy.

4. The estimated AlSiTiMgCrMn alloy produced using CrO_3 as the Cr-source and metallic Al as the reducing agent has the configurational entropy value of 1.52. The metal recoveries were calculated as 43.1% Cr, 28.4% Ti, and 21.31% Mn. This L-HEA is composed of a multiphase microstructure and could not be produced in equiatomic composition, and a homogeneous structure is not composed. According to XRD analysis, this L-HEA contained four phases: $Ti_7Al_5Si_{12}$, $Al10Mn_3$, Cr_3Si (A15), and $TiMnSi_2$. The obtained hardness value was calculated as 803.2 HV. It is thought that the formation of phases containing Mn causes the hardness values to decrease.

5. The estimated AlSiTiMgCrMnFe alloy produced using Cr_2O_3 as the Cr-source and metallic Al as the reducing agent has the configurational entropy value of 1.67. The metal recoveries were calculated as 99.6% Fe, 76.6% Cr, 56.2% Ti, and 37.4% Mn. According to XRD analysis, this L-HEA comprises six different phases: Al_8Mn_5, $AlMn_{0.75}Fe_{2.25}$, $Mn_4Ti_2Si_5$, and $MgAl_2O_4(H1_1)$, Al_3SiCr, and $CrFe_8Si$. The obtained hardness value is 907.8 HV. Fe element improved the hardness of AlSiTiMgCrMn alloy. It was determined that a higher hardness value was obtained in the alloy using Cr_2O_3 when the effect of using different Cr oxide raw materials on hardness was examined.The estimated AlSiTiMgCrMnFe alloy produced using CrO_3 as the Cr-source and metallic Al as the reducing agent has the highest configurational entropy value

of 1.70. The metal recoveries are calculated as 59.7% Fe, 48.1% Cr, 30% Ti, and 20.3% Mn. The equiatomic composition and a homogeneous structure were not obtained in this L-HEA. XRD analysis showed that five different phases were included in this L-HEA: $CrFe_8Si$, Al_8Mn_5, $AlMn_{0.75}Fe_{2.25}$, $Cr_{0.78}Fe_{2.22}Si_2$, and $Mn_4Ti_2Si_5$. The obtained hardness value is 896.2 HV.

In the direction of results obtained from this Master's thesis, it is recommended to apply heat treatment and secondary melting processes to improve the casting microstructures in future studies.

REFERENCES

Arons, B. (1992). A review of the cocktail party effect, *Journal of the American Voice I/O Society*, (12), 35–50.

Biswas, A., Roy, S. K., Gurumurthy, K. R., Prabhu, N., & Banerjee, S. (2002). A study of self-propagating high-temperature synthesis of NiAl in thermal explosion mode, *Acta Materialia*, (59), 757–773.

Cantor, B., Chang, I., Knight, P., & Vincent, A. (2004). Microstructural development in equiatomic multicomponent alloys. *Materials Science and Engineering: A*, 375-377, 213-218.

Chang, S.Y., Lin, S.Y., Huang, Y.C., Wu, C.L. (2010). Mechanical properties, deformation behaviors and interface adhesion of $(AlCrTaTiZr)N_x$ multi-component coatings. *Surface and Coatings Technology*, *204*(20), 3307-3314.

Crider, J. F. (1982). Self-propagating high temperature synthesis – A Soviet method for producing ceramic materials. In W. J. Smothers (Ed.), *Ceramic Engineering and Science Proceedings*, 519-528.

Cullity, B. D., & Stock, S. R. (2001). "Elements of x-ray diffraction," *Upper Saddle River: NJ: Prentice-Hall Inc.* (3rd ed.), 57-63.

Del Grosso, M. F., Bozzolo, G., & Mosca, H. O. (2012). Determination of the transition to the high entropy regime for alloys of refractory elements. *Journal of alloys and compounds*, (534), 25-31.

Detrois, M., Antonov, S., & Tin, S. (2019). Phase stability and thermodynamic database validation in a set of non-equiatomic Al-Co-Cr-Fe-Nb-Ni high-entropy alloys. *Intermetallics*, (104), 103–112.

Gao, M., Yeh, J., Liaw, P., & Zhang, Y. (2016). High-Entropy Alloys. *Cham: Springer International Publishing*, *8*(2), 1-512.

Gao, M.C., Yeh, J.W., Liaw, P.K., & Zhang, Y. (2014). Overview of high-entropy alloys. *High-Entropy Alloys: Fundamentals and Application*, 4-52.

Gaskell, D. R. (2003). *Introduction to the Thermodynamics of Materials*," London, UK.: Taylor and Francis (4th ed.), 89-92.

Gludovatz, B., Hohenwarter, A., Catoor, D., Chang, E. H., George, E. P., & Ritchie, R. O. (2014). A fracture-resistant high-entropy alloy for cryogenic applications. *Science, 345*(6201), 1153–1158.

Hammond, V. H., Atwater, M. A., Darling, K. A., Nguyen, H. Q., Kecskes, L. J. (2014). Equal-channel angular extrusion of a low-density high-entropy alloy produced by high-energy cryogenic mechanical alloying. *JOM*, (66), 2021-2029.

Hislrey, F. C., & Jean, A. (1956). Lamoureux, continuous process for metallothermic reactions, Application April 30, Serial No. 581,343 16 Claims. (Cl. 75-27).

Hsu, C. Y., Wang, W. R., Tang, W. Y., Chen, S. K., & Yeh, J. W. (2010). Microstructure and mechanical properties of new $AlCo_xCrFeMo_{0.5}Ni$ high-entropy alloys. *Advanced Engineering Materials, 12*(1-2), 44-49.

Huang, K. H., & Yeh, J. W. (1996). A study on the multicomponent alloy systems containing equal-mole elements. *M.S. thesis*, Hsinchu: National Tsing Hua University, 1.

Hyun, J. I., Kong, K. H., Kim, K. C., Kim, W. T., & Kim, D. H. (2015). Microstructural evolution in CuCrFeNi, CuCrFeNiMn, and CuCrFeNiMnAl high entropy alloys. *Applied Microscopy, 45*(1), 9-15.

Inoue, A. (2000). Stabilization of metallic supercooled liquid and bulk amorphous alloys. *Acta Materialia,* (48), 279-306.

Inoue, A., & Gook, J. S. (1995). Fe-based ferromagnetic glassy alloys with wide supercooled liquid region. *Materials Transactions, JIM, 36*(9), 1180-1183.

Joseph, J., Stanford, N., Hodgson, P., & Fabijanic, D. M. (2017). Understanding the mechanical behaviour and the large strength/ductility differences between FCC and BCC $Al_xCoCrFeNi$ high entropy alloys. *Journal of Alloys and Compounds*, (726), 885-895.

Kitain, E. I., Kitain, M. M., & Sukhovitskaya, E. A. (1978). Report GIPKh 3-78.

Li, R., Gao, J. C., Fan K. (2011). Microstructure and mechanical properties of MgMnAlZnCu high entropy alloy cooling in three conditions. *Materials Science Forum*, (686), 235-241.

Li, R., Gao, J. C., Fan, K. (2010). Study to microstructure and mechanical properties of Mg containing high entropy alloys. *Materials Science Forum*, (650), 265-271.

Li, Y., Zhang, Y. (2019). Light-weight and flexible high-entropy alloys., *Engineering Steels and High Entropy-Alloys*, Chapter 7, 1-11.

Liu, W. H., Wu, Y., He, J. Y., Nieh, T. G., & Lu, Z. P. (2013). Grain growth and the Hall–Petch relationship in a high-entropy FeCrNiCoMn alloy. *Scripta Materialia*, *68*(7), 526-529.

Liu, Y. Y., Chen, Z., Shi, J. C., Wang, Z. Y., & Zhang, J. Y. (2019). The effect of Al content on microstructures and comprehensive properties in $Al_xCoCrCuFeNi$ high entropy alloys. *Vacuum*, (161), 143–149.

Mamyan, S. S., Petrov, Y. M., & Stesik, L. N. (1975). *Combustion Processes in Chemical Technology and Metallurgy*. Chernogolovka, 188.

Mamyan, S. S., Shiryaev, A. A., & Merzhanov, A. G. (1993). Inorganic materials by shs with a reduction stage: thermodynamic study. *Journal of Engineering Physics and Thermophysics*, *65*, 431-438.

Merzhanov, A. G. (1967). Thermal explosion and ignition as a method for formal kinetic studies of exothermic reactions in the condensed phase. *Combustion and Flame, 11*(3), 201-211.

Merzhanov, A. G. (1990). Combustion and plasma synthesis of high-temperature materials. New York: VHC 1.

Merzhanov, A. G. (1995). History and recent developments in SHS. *Ceramics International, 21*(5), 371-379.

Merzhanov, A. G. (2002). *Self-propagating High-temperature Synthesis* (SHS), ISMAN, Russia. (5), 301-322.

Merzhanov, A. G. (2012). Results of 40-year development. In A. G. Merzhanov (Ed.), *40 Years of SHS: A Lucky Star of a Scientific Discovery*, 69-89.

Merzhanov, A. G., & Sytchev, A. E. (2002). SHS in microgravity. In A. A. Borisov, L. De Luca and A. Merzhanov (Eds.), *Self-Propagating High-Temperature Synthesis of Materials*, 301-322.

Merzhanov, A. G., Shkiro, V. M., & Borovinskaya, I. P. (1973). Method of producing refractory carbides, borides, silicides, sulfides, and nitrides of metals of groups IV, V, and VI of the periodic system, United State Patent, No: 3726643**.**

Miracle, D. B., & Senkov, O. N. (2017). A critical review of high entropy alloys and related concepts. *Acta Materialia*, (122), 448-511.

Miracle, D., & Senkov, O. (2017). A critical review of high entropy alloys and related concepts. *Acta Materialia*, (122), 448-511.

Mishra, S. S., Yadav, T. P., Srivastava, O. N., Mukhopadhyay, N. K., & Biswas, K. (2020). Formation and stability of C14 type Laves phase in multi component high-entropy alloys. *Journal of Alloys and Compounds*, (832), 1-7.

Mossino, P. (2004). Some Aspects in Self-Propagating High-Temperature Synthesis, *Ceramics International*, Turin, Italy. *30*(3), 311-332.

Munir, Z. A., & Tamburini, U. A. (1989). Self-propagating exothermic reactions: the synthesis of high-temperature materials by combustion, *Materials Science Reports*, *3*(6), 277–358.

Murty, B. S., & Yeh, J. W., Ranganathan, S., & Bhattacharjee, P. P. (2019). "High-entropy alloys: basic concepts," *High-Entropy Alloys*, 13–30.

Murty, B., Yeh, J., & Ranganathan, S. (2014). *High-Entropy Alloys.* (1st ed.) San Diego: Elsevier. 1-218.

Murty, B.S., Yeh, J.W., Ranganathan, S. (2014). *High-Entropy Alloys*, Chapter 1- A Brief History of Alloys and the Birth of High-Entropy Alloys. Oxford, UK: Butterworth-Heinemann, 1-12.

Ng, C., Guo, S., Luan, J., Shi, S., & Liu, C. T. (2012). Entropy-driven phase stability and slow diffusion kinetics in an $Al_{0.5}$CoCrCuFeNi high entropy alloy. *Intermetallics*, *31*, 165-172.

Pradeep, K., Tasan, C., Yao, M., Deng, Y., Springer, H., & Raabe, D. (2015). Non-equiatomic high entropy alloys: approach towards rapid alloy screening and property-oriented design. *Materials Science and Engineering: A, 648*, 183-192.

Ranganathan, S. (2003). Alloyed pleasures: multimetallic cocktails. *Current science, 85*(5), 1404-1406.

Senkov, O. N., & Miracle, D. B. (2001). Effect of the atomic size distribution on glass forming ability of amorphous metallic alloys. *Materials Research Bulletin*, *36*(12), 2183–2198.

Senkov, O. N., Miracle, D. B., Chaput, K. J., & Couzinie, J.-P. (2018). Development and exploration of refractory high entropy alloys—A review. *Journal of Materials Research*, *33*(19), 3092–3128.

Senkov, O. N., Wilks, G. B., Miracle, D. B., Chuang, C. P., & Liaw, P. K. (2010). Refractory high-entropy alloys. *Intermetallics*, *18*(9), 1758–1765.

Shewmon, P., & Gill, C. (2018). Approach to self healing in metal matrix composites: A review. *Materials Today: Proceeding,* (5), 19703–1971.

Singh, S., Wanderka, N., Murty, B. S., Glatzel, U., & Banhart, J. (2011). Decomposition in multi-component AlCoCrCuFeNi high-entropy alloy. *Acta Materialia*, *59*(1), 182-190.

Stepanov, N.D., Yurchenko, N. Yu., Shaysultanov, D. G., Salishchev, G. A. & Tikhonovsky, M. A. (2015). Effect of Al on structure and mechanical properties of $Al_xNbTiVZr$ (x = 0, 0.5, 1, 1.5) high entropy alloys. *Materials Science and Technology*, (31), 1184-1193.

Stepanov, N.D., Yurchenko, N.Y., Skibin, D.V., Tikhonovsky, M.A., Salishchev, G.A. (2015). Structure and mechanical properties of the $AlCr_xNbTiV$ (x = 0, 0.5, 1, 1.5) high entropy alloys. *Journal of Alloys and Compounds,* (652), 266-288.

Suryanarayana, C. (2001). "Mechanical alloying and milling," *Progress in Materials Science*, *46*(1-2), 1–184.

Takeuchi, A., & Inoue, A. (2000). Calculations of mixing enthalpy and mismatch entropy for ternary amorphous alloys. *Materials transactions, JIM*, *41*(11), 1372-1378.

Tarakanov, A. Y., Shiryaev, A. A., Yukhvid, V. I., & Vzryva, G. F. (1991). Combustion, *Explosion and Shock waves*, (27), 68.

Tong, C. J., Chen, M. R., Yeh, J. W., Lin, S. J., Chen, S. K., Shun, T. T., & Chang, S. Y. (2005). Mechanical performance of the $Al_xCoCrCuFeNi$ high-entropy alloy system with multiprincipal elements. *Metallurgical and Materials Transactions A*, *36*(5), 1263-1271.

Tong, C. J., Chen, M. R., Yeh, J. W., Lin, S. J., Chen, S. K., Shun, T. T., & Chang, S. Y. (2005). Mechanical performance of the $Al_xCoCrCuFeNi$ high-entropy alloy system with multiprincipal elements. *Metallurgical and Materials Transactions A*, *36*(5), 1263-1271.

Tong, C. J., Chen, Y. L., Yeh, J. W., Lin, S. J., Chen, S. K., Shun, T. T., & Chang, S. Y. (2005). Microstructure characterization of $Al_xCoCrCuFeNi$ high-entropy

alloy system with multiprincipal elements. *Metallurgical and Materials Transactions A, 36*(4), 881-893.

Tsai, C. W., Tsai, M. H., Yeh, J. W., & Yang, C. C. (2010). Effect of temperature on mechanical properties of $Al_{0.5}CoCrCuFeNi$ wrought alloy. *Journal of Alloys and Compounds, 490*(1-2), 160-165.

Tsai, K. Y., Tsai, M. H., & Yeh, J. W. (2013). Sluggish diffusion in Co–Cr–Fe–Mn–Ni high-entropy alloys. *Acta Materialia*, *61*(13), 4887-4897.

Tsai, M. H. & Yeh, J. W. (2014). "High-entropy alloys: A critical review," *Materials Research Letters*, *2*(3), 107–123.

Tseng, K., Yang, Y.C., JUAN, C.C., Chin, T.S., Tsai, C.W., Yeh, J.W. (2018), A light-weight high-entropy alloy $Al_{20}Be_{20}Fe_{10}Si_{15}Ti_{35}$, *Science China Technological Sciences*, (61), 184-188.

Varna, A., & Mukasyan, A. S. (2002). Combustion synthesis of intermetallic compounds. In A. A. Borisov, L. De Luca and A. Merzhanov (Eds.), *Self-Propagating High-Temperature Synthesis of Materials*, 1-34.

Winter, M. (2020, October 16) *The periodic table of the elements*. https://www.webelements.com/

Xu, D.K., Han, E.H. (2012). Effects of icosahedral phase formation on the microstructure and mechanical improvement of Mg alloys: A review. *Progress in Natural Science: Materials International*, *22*(5), 364-385.

Yang X., Zhang, Y., Liaw, P.K. (2012). Microstructure and compressive properties of $NbTiVTaAl_x$ high entropy alloys, *Procedia Engineering*, (36), 292-298.

Yang, J.J., Chia-Ming Kuo, C.M., Lin P.T., Liu H.C., Huang, C.Y., Yen, H.W., Tsai, C.W. (2020). Improvement in oxidation behavior of $Al_{0.2}Co_{1.5}CrFeNi_{1.5}Ti_{0.3}$ highentropy superalloys by minor Nb addition, *Journal of Alloys and Compounds*, (825), 1-8.

Yang, X., Chen, S. Y., Cotton, J. D. & Zhang, Y. (2014). Phase stability of low-density, multiprincipal component alloys containing Aluminum, Magnesium, and Lithium, *JOM*, (66), 2009-2020.

Yeh, J. (2006). Recent progress in high-entropy alloys. *Annales de Chimie Science des Matériaux*, *31*(6), 633-648.

Yeh, J. W. (2013). "Alloy design strategies and future trends in high-entropy alloys," *JOM*, *65*(12), 1759–1771.

Yeh, J., Chen, S., Lin, S., Gan, J., Chin, T., Shun, T., Tsau, C., & Chang, S. (2004). Nanostructured high-entropy alloys with multiple principal elements: novel alloy design concepts and outcomes. *Advanced Engineering Materials*, *6*(5), 299-303.

Zhang, Y., Zuo, T. T., Tang, Z., Gao, M. C., Dahmen, K. A., Liaw, P. K., & Lu, Z. P. (2014). Microstructures and properties of high-entropy alloys. *Progress in Materials Science*, (61), 1-93.

Zhang, Y., Zuo, T.T., Tang, Z., Gao, M.C., Dahmen, K.A., Liaw, P.K., Lu, Z.P. (2014). "Microstructures and properties of high-entropy alloys," *Progress in Materials Science*, (61), 1–93.

Zhou, Y. J., Zhang, Y., Wang, Y. L., & Chen, G. L. (2007). Solid solution alloys of $AlCoCrFeNiTi_x$ with excellent room-temperature mechanical properties. *Applied physics letters*, *90*(18), 181-904.